Lithos 382–383 (2021) 105957

Contents lists available at ScienceDirect

Lithos

journal homepage: www.elsevier.com/locate/lithos

Research Article

Zircon from the Chuktukon alkaline ultramafic carbonatite complex (Chadobets uplift, Siberian craton) as evidence of source heterogeneity

A.G. Doroshkevich [a,b,*], V.V. Sharygin [a,c,d], E.A. Belousova [e], I.A. Izbrodin [b], I.R. Prokopyev [a,c]

[a] V.S.Sobolev Institute of Geology and Mineralogy, Siberian Branch of the Russian Academy of Sciences, Novosibirsk, Russia
[b] Geological Institute, Siberian Branch of the Russian Academy of Sciences, Ulan-Ude, Russia
[c] Department of Geology and Geophysics, Novosibirsk State University, Novosibirsk, Russia
[d] ExtraTerra Consortium, Institute of Physics and Technology, Ural Federal University, 19 Mira str., Ekaterinburg 620002, Russia
[e] Department of Earth and Environmental Sciences, Macquarie University, Sydney, NSW 2109, Australia

ARTICLE INFO

Article history:
Received 7 July 2020
Received in revised form 21 December 2020
Accepted 22 December 2020
Available online 26 December 2020

Keywords:
Zircon
Geochronology
Hf isotopes
Multiphase inclusions
Carbonatite
Damtjernite
Alkaline ultramafic magmatism
Chadobets uplift

ABSTRACT

The Chuktukon alkaline carbonatite complex is a part of the Chadobets complex, situated in the southwestern part of the Siberian craton. It is composed principally of aillikite-damtjernite and carbonatite and a host of Nb and REE mineralisation. Zircons were collected from drillhole samples of the damtjernites and hydrothermally overprinted carbonatites. Zircon grains show oscillatory zoning and a significant signature of recrystallization in cathodoluminescence images. Oscillatory zoned zircons preserved primary signatures, whereas recrystallization processes were related to infiltration of carbonatite melt and late stage fluid. The recrystallization led to different changes in the zircon geochemistry and appearance of multiphase inclusions with mineral composition, which is common of carbonatites (alkali-rich carbonates, fluorcalciopyrochlore, fluorapatite, Ba-Sr-REE-Ca-carbonates, calcite, dolomite, phlogopite and others). Hf-isotope composition of oscillatory zoned and recrystallized zircons is similar and records the signature of their primary heterogeneous source, with εHf(t) varying from 6.3 to −0.6. U-Pb age of oscillatory zoned zircon from damtjernite shows that the rock was emplaced at 256.7 ± 1.1 Ma, indicating that the Chuktukon intrusion was coeval with the Permian-Triassic Siberian Traps (252–250 Ma) and extensive alkaline magmatism in the Siberian craton.

1. Introduction

Kimberlites, carbonatites, lamproites and ultramafic lamprophyres are among the most extreme partial melting products of the Earth's mantle that are enriched in volatiles, REE and trace elements. In addition, mantle-derived alkaline magmatism is rare on the surface. In spite of their minor surface occurrence, the alkaline rocks are important components of the large igneous provinces related to mantle plumes (e.g. Ernst et al., 2018; Rao and Lehmann, 2011).

The Siberian craton was the site of extensive magmatic activity at the Permian-Triassic period, including eruption of one of the largest continental flood basalt provinces on the Earth with only minor occurrences of alkaline basalts, meimechites, kimberlites, carbonatites and ultramafic lamprophyres. The temporal association of alkaline magmatism with the Siberian traps provides an opportunity to investigate the compositional heterogeneity in the mantle beneath the Siberian craton and the variety of involved primary magmas.

Recent petrologic and Sr-Nd-Pb-Hf isotope studies on the Maimecha-Kotuy alkaline rocks, Triassic Siberian kimberlites and Chadobets alkaline ultramafic carbonatite complex have revealed that they are produced from primary melts derived from a moderately depleted mantle (Arndt et al., 1998; Carlson et al., 2006; Doroshkevich et al., 2019; Fedorenko et al., 2000; Ghobadi et al., 2018; Kogarko and Zartman, 2011; Nosova et al., 2020; Sun et al., 2014, 2018), whereas the Siberian traps record continental lithospheric signatures in the basalt source (e.g., Carlson et al., 2006; Fedorenko et al., 2000; Lightfoot et al., 1993; Sharma et al., 1991, 1992; Wooden et al., 1993). On the other hand, Sr-Nd isotopic compositions of the Siberian traps and alkaline rocks lie on a linear trend that indicates their petrogenetic connection and relationship with the Siberian mantle superplume.

The study of U-Pb and Lu-Hf isotopes and trace-element geochemistry in zircons presents a unique opportunity to assess the composition of the primary sources and gain insight into processes in the Earth's deep mantle. We have obtained the first combined information on inclusions and trace-element concentration data, and U-Pb and Lu-Hf isotope composition of zircons derived from damtjernites and carbonatites of the Chuktukon complex, which is a part of the Chadobets alkaline ultramafic carbonatite complex.

* Corresponding author at: V.S.Sobolev Institute of Geology and Mineralogy, Siberian Branch of the Russian Academy of Sciences, Novosibirsk, Russia.
E-mail address: doroshkevich@igm.nsc.ru (A.G. Doroshkevich).

https://doi.org/10.1016/j.lithos.2020.105957
0024-4937/

2. Geological background

2.1. The Chadobets uplift and ultramafic alkaline carbonatite magmatism

The Chuktukon alkaline ultramafic carbonatite complex is located within the Chadobets uplift (basin of the Chadobets River, Krasnoyarsk Territory, Russia) at the southwestern part of the Siberian craton (Fig. 1). The uplift is 2000 km^2 in size and occurs at the intersection of two Neoproterozoic grabens, which are a part of the Angara-Kotuy large-scale rift system (Fig. 1) (Dashkevich, 1999; Staroseltsev, 2009). In addition to Chuktukon, the Chadobets uplift also includes the Terina complex. Both, Terina and Chuktukon, are combined into the Chadobets alkaline ultramafic carbonatite complex. The Chadobets complex comprises ultramafic lamprophyres (the rocks are classified as aillikite-damtjernite series based on the mineralogical composition and the classification scheme established by Tappe et al. 2005) and

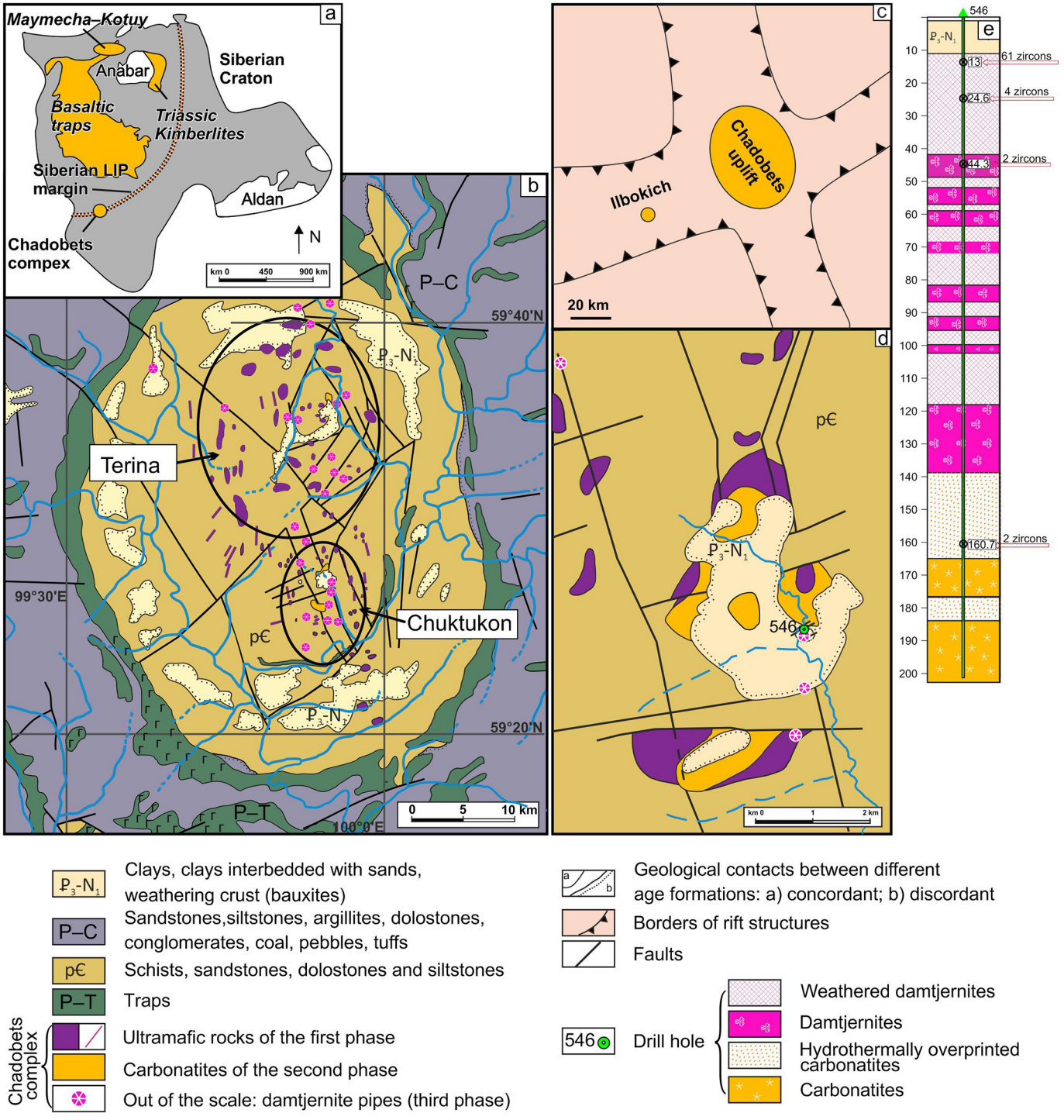

Fig. 1. (a) Location of the Chadobets alkaline ultramafic carbonatite complex within the Siberian Large Igneous Province (LIP) (after Pernet-Fisher et al., 2015); (b) Geological scheme of the Chadobets uplift (after Kirichenko et al., 2012); (c) Location of the Chadobets uplift within of two Neoproterozoic grabens (Angara-Kotuy rift system) (after Dashkevich, 1999; Staroseltsev, 2009); (d) Geological scheme of the Chuktukon complex (unpublished data from geological report of "Krasnoyarskgeols'emka", 2010) with marked 546 drillhole, from which zircon samples were collected; (e) profile of 546 drillhole with points of zircon sampling.

carbonatites. The carbonatites and their weathered crust host major reserves of Nb and REE (Lomayev and Serdyuk, 2011).

Previously reported U-Pb and Ar-Ar ages for the Chadobets ultramafic alkaline rocks and carbonatites are between 252 and 231 Ma (Chebotarev et al., 2017a; Nosova et al., 2020).

It is important to note, that the 392 Ma Ilbokich aillikite-damtjernite series is located nearby to the Chadobets uplift (Kargin et al., 2016; Nosova et al., 2018, 2020) (see Fig. 1).

The detailed geology of the Chadobets alkaline ultramafic carbonatite complex was described by Kirichenko et al. (2012). The sequence of the Chuktukon rocks, from the oldest to the youngest, was established by field observations (drillholes logs) and comprises alkaline ultramafic rocks, carbonatites and, finally, damtjernites (e.g. Kirichenko et al., 2012 and references in therein). Alkaline ultramafic rocks (aillikites-damtjernites, olivine melilitite, peridotite and others) of the first emplacement phase form small plugs (up to 1–1.5 km^2), dykes and sills ranging in thickness up to 100–120 m. Carbonatites also form small plugs (up to 4 km^2), dykes and sills (up to 20 m thick). Damtjernites are represented by pipes (up to 0.5 km^2), crosscutting early phase of alkaline ultramafic rocks and carbonatites and typically containing their xenoliths. All rocks of the Chuktukon complex are intensely altered by hydrothermal and weathering processes (e.g. Kirichenko et al., 2012 and references in therein).

The petrography and mineralogy of the Chadobets alkaline rocks were studied in detail by Kirichenko et al. (2012), Lapin (2001), Lapin and Lisitzyn (2004), Sharygin et al. (2016a, 2016b), Sharygin (2017), Chebotarev et al. (2017b), Nosova et al. (2018), Doroshkevich et al. (2019), Prokopyev et al. (2020) and others. A brief summary of the petrographic features of the Chuktukon rocks is given below.

Dykes of alkaline ultramafic rocks (aillikites) have microporphyritic textures; olivine (up to 20%), clinopyroxene (up to 10%) and phlogopite (up to 10%) microphenocrysts occur in a fine-grained matrix that is composed of perovskite (10%), phlogopite-kinoshitalite, clinopyroxene (10%), fluorapatite, dolomite (30%), spinel group minerals and Ca-garnet (andradite-grossular). Monazite-(Ce), zircon, Zr- and Nb-bearing rutile, ilmenite, calzirtite, sulphides (pentlandite), and titanite are accessory minerals. The secondary hydrothermal minerals are calcite, barite, quartz, serpentine-group minerals, chlorite-, cancrinite- and kaolinite group minerals, and romanéchite. Olivine, clinopyroxene and phlogopite microphenocrysts usually are altered. Alteration products of the olivine are calcite and serpentine-group minerals. Clinopyroxene is hedenbergite varietie, chlorite-group minerals partially replace the clinopyroxene and phlogopite. The spinel-group minerals occur as composite crystals where Cr-spinel cores are mantled by tiny Ti-magnetite rims with composition showing the "titanomagnetite trend" (Doroshkevich et al., 2019).

The damtjernites have porphyritic textures with large rounded-to-anhedral phlogopite, dolomite-ankerite and olivine macrocrysts (up to 30% of rock volume) as well as xenoliths (host sedimentary rocks, alkaline ultramafic rocks, carbonatite, peridotites and eclogites) set in a fine-grained matrix. The rocks are abundant in pelletal lapilli, in which the cores of the macrocrysts are surrounded by dolomite-K-feldspar microlithic material with K-feldspar and dolomite plates, and calcite, rutile, spinel, apatite and phlogopite micrograins (Doroshkevich et al., 2019). The matrix is composed of dolomite-ankerite (up to 40%), K-feldspar (up to 5%), phlogopite (up to 10–15%), perovskite and spinelgroup minerals (up to 5–7%) with minor and accessory fluorapatite, sulphides, ilmenite, monazite-(Ce), zircon, Zr- and Nb-bearing rutile and fluorcalciopyrochlore. Secondary minerals are quartz, calcite, kaolinite-group minerals, strontianite, daqingshanite-(Ce) and barite. Dolomite-calcite-quartz aggregate replace the olivine macrocrysts. Cr-spinel occurs as discrete euhedral crystals and exhibits an atoll texture surrounded by thin rings of Ti-magnetite, their mineral compositions are consistent to the "titanomagnetite trend" (Doroshkevich et al., 2019). Macrocrysts of phlogopite are enriched in TiO_2 (up to 8 wt%) and Cr_2O_3 (up to 1.6 wt%), whereas the groundmass micas are enriched in F (4.5 wt%) and depleted in TiO_2 (up to 2 wt%) and Cr_2O_3 (bdl). Composition of the groundmass micas are consistent with the Al-enrichment trends for orangeites and ultramafic lamprophyres (Doroshkevich et al., 2019).

Carbonatites are massive fine- to medium-grained rocks with massive, spotty and banded textures. Calcite is the predominant groundmass mineral. The most abundant non-carbonate minerals of the carbonatite are tainiolite, fluorapatite, and fluorcalciopyrochlore with grains reaching several mm in size. Rippite, fluorite, Nb-rich rutile, K-feldspar, aegirine, ancylite-(Ce), strontianite, olekminskite, sulphides, and zircon are common minor and accessory mineral phases. Barite, quartz, goethite, Sr-rich carbonate-fluorapatite, Ca-REE-fluorcarbonates (parisite-(Ce), synchysite-(Ce)), monazite-(Ce), Sr-Ba-Pb-rich hydropyrochlore and romanèchite-hollandite aggregates are associated with the late hydrothermal stage.These minerals occur interstitially among the primary mineral grains and/or form networks of microveinlets. Calcite is speckled with dolomite spots and fine disseminations of ancylite-(Ce), strontianite, and olekminskite (Sharygin et al., 2016a).

2.2. Zircon samples

We studied 69 zircon grains that were recovered from crushed samples from drillhole (no. 546) of the Chuktukon complex (Figs. S1 and S2). It should be noted that zircon is a rare accessory mineral in the Chuktukon rocks and was found only in the following depths of the drillhole (in meters): 13 – highly weathered damtjernites (61 grains); 24.6 – weathered damtjernites (4 grains); 44.3 – damtjernites (2 grains); 160.7 – hydrothermally overprinted carbonatites (2 grains). All zircon fragments are smaller than 1–2 mm in size. Some zircon grains are characterized by a combination of short prismatic and bipyramidal crystal faces or irregular shapes. Most grains are transparent to semi-transparent and light yellow to honey-yellowish in colour. Prior to analytical isotope work, polished surfaces were examined for zoning and cathodoluminescent images were taken on the electron microprobe by the irradiation of the zircon with the electron beam with operating conditions of 15 kV accelerating voltage and 15–20 nA beam current at Macquarie University, Australia.

Typical cathodoluminescent (CL) and back-scattered electron (BSE) images of zircons are shown in Supplementary Fig. S2 a, b. Some studied zircon grains show oscillatory zoning on CL images indicative of their magmatic origin. Other samples are characterized by a complex structure in CL images, with a combination of oscillatory zoning and significant number of lighter domains developed along microcracks and rims of grains that testify new zircon overgrowths and local recrystallization.

Multiphase and monomineralic inclusions have been observed and studied in all zircon grains, whereas trace elements and Hf isotopic compositions were analysed in 34 and 30 grains, respectively. A total of 32 zircons were U-Pb dated.

3. Analytical methods

3.1. U-Pb dating and trace-element analysis

The zircons have been U-Pb dated by LAM-ICPMS technique at Macquarie University, Australia. The analyses were carried out using Agilent 7700 quadrupole ICP-MS instruments, attached to a Photon Machines Excimer 193 nm laser system. The analyses were carried out with a beam diameter of ca 30–40 μm with 5 Hz repetition rate and energy of around 0.06 μJ and 8 J/cm^2. The analytical procedures for the U-Pb dating have been described in detail previously (Jackson et al., 2004). A very fast scanning data acquisition protocol was employed to minimise signal noise. Data acquisition for each analysis took three minutes (one minute on background, two minutes on signal). Ablation was carried out in He to improve sample transport efficiency, provide more stable signals and give more reproducible Pb/U fractionation. Provided that

constant ablation conditions are maintained, accurate correction for U/Pb fractionation can then be achieved using an isotopically homogeneous zircon standard.

Samples were bracketed at the beginning and the end by pairs of analyses of the GEMOC GJ-1 zircon standard (Elhlou et al., 2006). This standard is slightly discordant, and has a TIMS $^{207}Pb/^{206}Pb$ age of 608.5 Ma (Jackson et al., 2004). The other well-characterized zircon standard 91,500 and Mud Tank were analysed within the run as an independent control on reproducibility and instrument stability. The data collected for the 91,500 and Mud Tank zircons are available in the spreadsheet (Supplementary file TC-178 workbook and sheets with 91,500 and Mud Tank data). The average values for these standards accordingly: $^{207}Pb/^{206}Pb$ age of 1065 ± 10 Ma (1sd, $n = 4$) for 91,500, and $^{206}Pb/^{238}U$ age of 740 ± 5 Ma (1sd, n = 4) for Mud Tank. The Temora zircon ($^{206}Pb/^{238}U$ age of 418 ± 5 Ma (1sd, n = 4)) was also analysed, its $^{206}Pb/^{238}U$ IDTIMS age has been determined to be 416.75 ± 0.24 Ma (Black et al., 2003).

U-Pb ages were calculated from the raw signal data using the online software package GLITTER (www.mq.edu.au/GEMOC; Griffin et al., 2008). GLITTER calculates the relevant isotopic ratios for each mass sweep and displays them as time-resolved data. This allows isotopically homogeneous segments of the signal to be selected for integration. GLITTER then corrects the integrated ratios for ablation related fractionation and instrumental mass bias by calibration of each selected time segment against the identical time segments for the standard zircon analyses.

For zircon analyses we have employed the common-Pb correction procedure of Andersen (2002) and the analyses presented here have been corrected assuming recent lead-loss with a common-lead composition corresponding to present-day average orogenic lead as given by the second-stage growth curve of Stacey and Kramers (1975) for $^{238}U/^{204}Pb = 9.74$. No correction has been applied to analyses that are concordant within 2σ analytical error in $^{206}Pb/^{238}U$ and $^{207}Pb/^{235}U$, or which have less than 0.2% common lead.

3.2. Hf-isotope analysis

Hf-isotope analyses were carried out in the Geochemical Analysis Unit of the GEMOC/CCFS Centre in the Department of Earth and Planetary Sciences, Macquarie University. The details of the methodology and analytical condition for Lu-Hf isotope analysis are provided by Griffin et al. (2000). Hf-isotope analyses were carried out in-situ using a New Wave/Merchantek UP-213 laser-ablation microprobe, attached to a Nu Plasma multi-collector ICPMS. The analyses were carried out with a beam diameter 40 μm and a 5 Hz repetition rate and typical ablation times ca 100 s. Helium carrier gas transported the ablated sample from the laser-ablation cell via a mixing chamber to the ICPMS torch.

Interference of ^{176}Lu on ^{176}Hf was corrected by measuring the intensity of the interference-free ^{175}Lu isotope and using $^{176}Lu/^{175}Lu = 0.02669$ (DeBievre and Taylor, 1993) to calculate $^{176}Lu/^{177}Hf$. Similarly, the interference of ^{176}Yb on ^{176}Hf has been corrected by measuring the interference-free ^{172}Yb isotope and using $^{176}Yb/^{172}Yb$ to calculate $^{176}Yb/^{177}Hf$. The appropriate value of $^{176}Yb/^{172}Yb$ was determined by spiking the JMC475 Hf standard with Yb, and finding the value of $^{176}Yb/^{172}Yb$ (0.58669) required to yield the value of $^{176}Hf/^{177}Hf$ obtained on the pure Hf solution. Detailed discussions regarding the overlap corrections for ^{176}Lu and ^{176}Yb are provided in Pearson et al. (2008). Precision and accuracy obtainable on the $^{176}Hf/^{177}Hf$ ratio are illustrated by analyses of standard zircons in Griffin et al. (2000) and Pearson et al. (2008). The typical 2SE precision on the $^{176}Hf/^{177}Hf$ ratios presented here is about 0.00002, equivalent to +0.7 εHf unit. The Mud Tank and Temora zircons were used as independent control on reproducibility and instrument stability. Most of the data and the mean value are within 2 s.d. of the recommended values reported for Mud Tank ($^{176}Hf/^{177}Hf = 0.282522 \pm 42$ (2sd), Griffin et al., 2007) and Temora reference material (0.282680 ± 15, Kemp et al., 2005).

For the calculation of εHf values, we have adopted the chondritic values of Bouvier et al. (2008): $^{176}Lu/^{177}Hf$ (CHUR, today) = 0.0336, $^{176}Hf/^{177}Hf$ (CHUR, today) = 0.282785 and the decay constant for ^{176}Lu of 1.865 × 10–11 yr-1 (Scherer et al., 2001). To calculate model ages (TDM) based on a depleted-mantle source, we assume that the depleted mantle (DM) reservoir developed from an initially chondritic mantle, and is complementary to the crust extracted over time. TDM ages, which are calculated using the measured $^{176}Lu/^{177}Hf$ of the zircon, can only give a minimum age for the source material of the magma from which the zircon crystallised. Therefore we have also calculated, for each zircon, a "crustal" Model age (TDMC in Data tables) which assumes that its parental magma was produced from an average continental crust ($^{176}Lu/^{177}Hf = 0.015$; Geochemical Earth Reference Model database, http://www.earthref.org/) that was derived from a depleted mantle.

3.3. Zircon trace-element analysis

Trace-element content was analysed using Agilent 7700 quadrupole ICP-MS instruments, attached to a Photon Machines Excimer 193 nm laser system at the GAU, Macquarie University. The analyses were carried out using the same laser condition as for U-Pb dating. Detailed descriptions of analytical and calibration procedures have been given by Belousova et al. (2002).

Zirconium content was used for internal calibration and quantitative results for the trace elements reported here were obtained through calibration of relative element sensitivities using the NIST-610 standard glass as the external calibration standard. The precision and accuracy of the NIST-610 analyses are 1–2% for REE, Y, Sr, Nb, Hf, Ta, Th and U at the ppm concentration level, and from 5% to 10% for Ca, P and Ti.

3.4. Petrography of inclusions

All studies of multiphase inclusions in zircon were performed in the Institute of Geology and Mineralogy, Novosibirsk, Russia. Optical examination of the samples (monitoring of multiphase inclusions) was performed using an Olympus BX51 microscope.

BSE images, elemental maps, and energy-dispersive spectroscopic (EDS) analyses of zircons and minerals from exposed inclusions were obtained using a MIRA 3LMU SEM (TESCAN Ltd.) equipped with an INCA Energy 450 XMax 80 microanalysis system (Oxford Instruments Ltd.). EDS analyses were done at an accelerating voltage of 20 kV, a probe current of 1 nA, and accumulation time of 20 s. The following simple compounds and metals were used as reference standards for most of the elements: SiO_2 (Si and O), Al_2O_3 (Al), diopside (Mg and Ca), albite (Na), orthoclase (K), $Ca_2P_2O_7$ (P), BaF_2 (Ba and F), Cr_2O_3 (Cr), pyrite (S), $CsRe_2Cl_6$ (Cl), metallic Ti, Fe, Mn, Zr, Hf and others. Correction for matrix effects was done using the XPP algorithm, implemented in the software of the microanalysis system. Metallic Co served for quantitative optimization (normalization to probe current and energy calibration of the spectrometer).

The Raman spectra of zircon and minerals from exposed multiphase inclusions were recorded on a LabRAM HR 800 mm (HORIBA Scientific Ltd.) spectrometer equipped with a 1024 pixel LN/CCD detector and coupled to an Olympus BX40 confocal microscope (objective x100). A semiconductor laser emitting at 514.5 nm with a nominal power output of 50 mW was used for excitation. In each case, 10–20 spectra were recorded for 10–20 s each at a hole diameter of 200 μm and integrated. Most spectra were recorded between 100 and 1200 cm^{-1}, and some spectra were made for the 100–4000 cm^{-1} and 3000–4000 cm^{-1} region. The monochromator was calibrated using the 520.7 cm^{-1} Raman line of elemental Si. The obtained spectra were compared with information from RRUFF database (Lafuente et al., 2016).

4. Results

4.1. Petrography of inclusions

Inclusions were found in all studied zircons. Minerals within inclusions were identified by EDS, elemental maps and Raman spectra. In general, all inclusions can be subdivided into multiphase and monomineralic species. The multiphase inclusions are rare in the studied zircons, whereas monomineralic ones are common and represented mainly by fluorapatite and carbonates, which are resistant to alteration process. The majority of zircon-hosted multiphase inclusions are altered and now represented by mixture of secondary minerals (kaolinite, Nb-rich goethite and unidentified Ba-Sr-Ca-REE-rich hydrated aluminophosphate). The chemical variations for the latter mineral are as follows (EDS, wt%): SiO_2–0.3-1.0, P_2O_5–24.1- 27.9, Al_2O_3–26.0-29.5, FeO – 0.2-2.4, CaO – 2.7-4.1, BaO – 5.8-8.5, SrO – 2.7-5.5, La_2O_3–1.6-2.8, Ce_2O_3–1.4-3.0, Nd_2O_3–0.9-1.4, F – 0.8-2.0. Some rare inclusions in the zircon interior are not altered and their sizes are not larger than 30 μm (Figs. 2-4).

Fluorapatite and calcite were found in zircons from the 24.6 m depth (weathered damtjernite), whereas Ca-Ba-carbonate was identified in zircons from the 44.3 m depth (fresh damtjernite). Rare inclusions were observed in the hydrothermally overprinted carbonatite from the 160.7 m depth. They are located in the core of the host zircon and, according to CL of zircons (Fig. S2a), seem to be secondary in origin in respect to the central parts of the host. In general they are carbonate-rich in composition and multiphase: calcite + dolomite or alkali-rich carbonates (nyerereite $Na_2Ca(CO_3)_2$ + shortite $Na_2Ca_2(CO_3)_3$ + burbankite $(Na,Ca)_3(Sr,Ba,Ce)_3(CO_3)_5$) (Fig. 2 and S2). The nyerereite phase contains >17.7 wt% Na_2O and >4.3 wt% K_2O.

Abundant monomineralic and multiphase inclusions were found in zircons of the upper horizon of the drillhole (the 13 m depth, highly weathered damtjernite, Figs. 3-4). Fluorapatite with 1.8–2.5 wt% SrO is dominant among monomineralic inclusions and commonly is present within growth zones in the host zircons (Fig. 3, Table S1). The pyrochlore-group minerals (U-, Th-, REE-rich species, from fluorcalciopyroclore to keno-hydropyrochlores), annite, ankerite and rutile sometimes occur as monomineralic inclusions (Figs. 3, S4 and S5, Tables S2 and S3). Some multiphase inclusions are confined to interior of zircon crystals (Fig. 3), but they are also secondary in origin according to CL of zircons (Fig. S2a). They are silicate-rich in compositions. One of such inclusions consists of albite, K-feldspar, annite $KFe^{2+}_3(AlSi_3O_{10})(OH,F)_2$, catapleiite $Na_2ZrSi_3O_9{\cdot}2H_2O$, a cancrinite-group mineral and minor calcite, dolomite, a pyrochlore-group mineral, sodalite $Na_8Al_6Si_6O_{24}Cl_2$, columbite-(Fe) and Na-rich zeolite (Figs. 3 and S6). Another inclusion contains magnesioarfvedsonite $(K_{0.27}Na_{0.73})(Na_{1.46}Ca_{0.54})(Mg_{3.10}Fe^{2+}_{1.36}Fe^{3+}_{0.32}Al_{0.10}Mn_{0.08}Ti_{0.05})(Al_{0.06}Si_{7.94})O_{22}(OH_{1.32}F_{0.68})$, ($n$ = 3, Table S3) and thorite $(Th,U)SiO_4$ (SiO_2–19.7-20.1; ThO_2–60.0-60.4; UO_2–1.6; PbO – 0.8-0.9 wt%) (Fig. 4).

One zircon grain (13-r3-Zr25, Fig. 4) is riddled with inclusions. They are secondary in origin and confined to healed fractures in the host zircon. Most of them are multiphase and sometimes contain gas bubble visible in transmitted light. Such inclusions are strongly variable in mineral composition: from silicate-carbonate to phosphate-carbonate and pure carbonate (Fig. 4B-I). Fluorine-rich phlogopite is dominant silicate within inclusions $K_{0.95}(Mg_{1.95}Fe^{2+}_{0.90}Mn_{0.07}Ti_{0.06}Al_{0.02})(Al_{0.94}Si_{3.06})O_{10}(OH_{1.07}F_{0.78}O_{0.15})$ (n = 4, Table S3). The weak deficiency of Al_2O_3 in this mica may suggest a light tendency towards tainiolite composition; considering that tainiolite $KMg_2Li(Si_4O_{10})F_2$ is common mineral of the Chuktukon calciocarbonatites (Sharygin, 2017) and calciocarbonatite fragments in damtjernite. Fluorapatite, nyerereite $Na_2Ca(CO_3)_2$, F-rich annite, calcite, burbankite-khanneshite $(Na,Ca)_3(Sr,Ba,Ce)_3(CO_3)_5$ - $(Na,Ca)_3(Ba,Sr,Ce,Ca)_3(CO_3)_5$ and Na-rich hydrated carbonate are common in phosphate-carbonate and pure carbonate inclusions (Figs. 4E-I, S7 and S8). Nyerereite phase contains up to 6.8 wt% K_2O.

4.2. U-Pb geochronology

11A total of 32 analyses were done for the zircons (Supplementary file TC-178 workbook), however the many of analyses are very discordant (> > 10%) or have a very large uncertainty due to the very low U content in some of the zircons (only several ppm) due to recrystallization process (see Section 4.3 and Discussion). Eight of most concordant oscillatory zoned grains with acceptable analytical precision have been used for age calculations, 2 out of those were rejected as outliers (much younger and older ages), and the final age was calculated using the remaining cluster of 6 analyses. The U-Pb isotope ratios and age results for the 6 analyses are provided in Supplementary Table S4 and presented in Fig. 5. Analysed grains are concordant and yield a weighted mean age of 256.7 ± 1.1 Ma (MSWD = 1.13) and this age might be attributed to the age of the Chuktukon damtjernites formation.

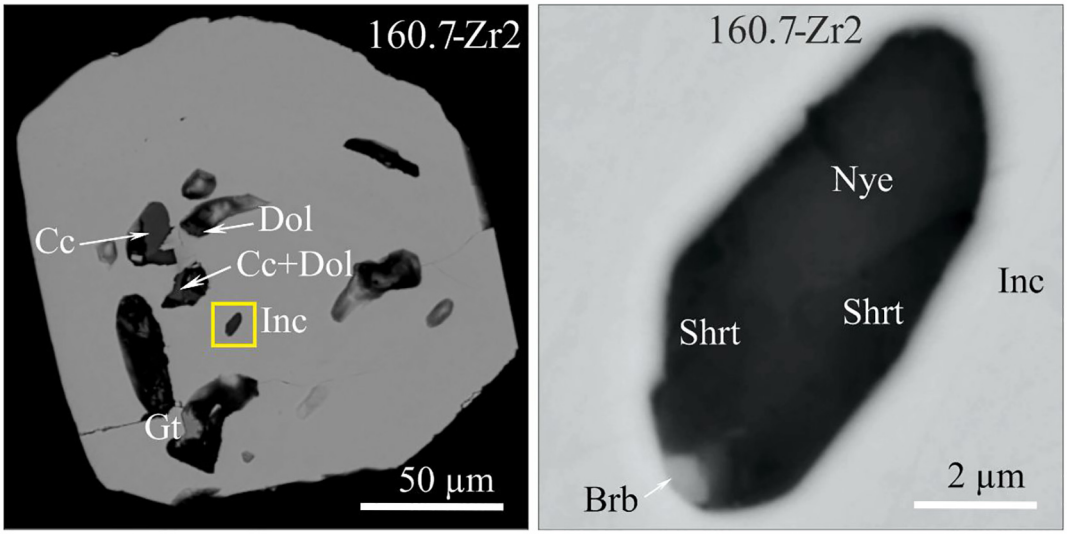

Fig. 2. Multiphase inclusions in zircon from altered calciocarbonatite (depth 160.7 m), BSE images. Cc – calcite, Dol – dolomite, Gt – goethite, Inc. – inclusion; Nye – nyerereite (?), Shrt – shortite, Brb – burbankite. Elemental maps and Raman data for the inclusion see Fig. S3.

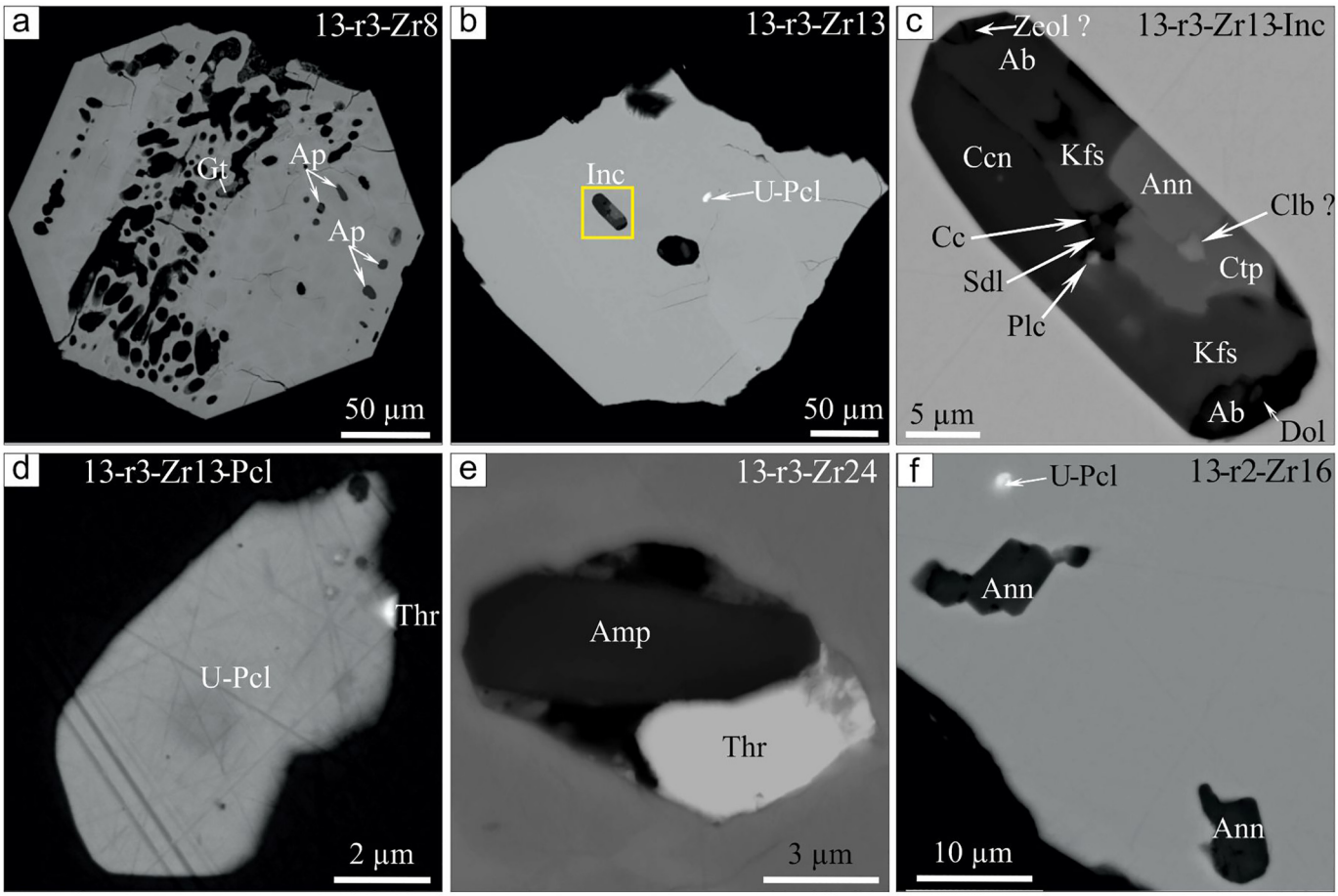

Fig. 3. Primary (?) multiphase inclusions in zircons from highly weathered damtjernite (depth 13.0 m), BSE images. Gt – goethite, Ap – fluorapatite, Inc. – inclusion, U-Pcl – U-rich oxycalciopyrochlore (UO_2 – up to 29 wt%), Cc – calcite, Ann – annite, Kfs – K-feldspar, Ab – albite, Ccn – a cancrinite-group mineral, Zeol? – Na-rich zeolite mineral (?), Sdl – sodalite, Pcl – a pyrochlore-group mineral, Ctp – catapleiite, Clb? – columbite-(Fe) (?), Thr – thorite, Amp – K-F-rich magnesioarfvedsonite. Elemental maps and Raman data for silicate inclusion see Fig. S5.

4.3. Trace-element compositions

A total of 34 trace-element analyses were done for the zircons, with the data provided in Supplementary Table S5. Discriminant diagrams with the range of some trace-element concentrations and the chondrite-normalized REE abundances are shown in Figs. 6 and 7.

Considering petrographic observation of inclusions, the entrapment of sub-micrometer monomineralic and multiphase inclusions (fluorapatite, pyrochlore, thorite, rutile and others) may be possible during the LA–ICP–MS analyses. However, 32 analyses display a relatively narrow range of P content (15–198 ppm), therefore excluding a presence of fluorapatite or aluminophosphate inclusions in analyzing areas. Nevertheless, the higher P, REE, Y, Nb and Ti contents (see Supplementary table S5 and Supplementary fig. S9) of one analysis (r1-160.7-1) may reflect the presence of sub-micrometer multiphase inclusions with phosphate and rutile or pyrochlore. A similar case is observed in the r1-24.6-2 sample, which may also indicate minor contamination by multiphase inclusions. Both analyses were excluded from trace-element results.

The normalized REE patterns of the zircons with oscillatory zoning (12 samples, see Fig. 6a and Supplementary Table S5) are characterized by positive Ce (3—22) anomaly with absent or slightly negative Eu (0.8–1) anomaly. REE concentrations vary from 352 to 1072 ppm, with Yb/Sm ratios =11–64. The patterns are similar to those of zircons from the carbonatite and lamproite (Fig. 6a) (Belousova et al., 2002), but the lamproite pattern shows a negative Eu anomaly that is consistent with the crystallization of feldspar.

Zircons with signatures of recrystallization and overgrowths can be divided into two distinct groups according to their REE patterns (Fig. 6). Type 1 analyses are characterized by low REE concentrations (14–69 ppm), steeply increasing chondrite-normalized REE patterns from Nd to Lu (La, Ce, Pr usually are below detection limits) with Yb/Sm ratios = 114–1377 and negative Eu anomalies ranging from 0.4 to 0.9. In contrast, type 2 analyses are characterized by much higher and strongly variable REE concentrations (142–2435 ppm). Eu anomaly ranges from 0.8 to 1.1. Ce anomaly (1–17) is similar to this of zircon with oscillatory zoning. Nevertheless, on the Ce/Ce* vs Eu/ Eu* diagram (see Fig. 7), most points of all zircon types are within fields characteristic of zircons from carbonatites, lamproites and kimberlites (Belousova et al., 2002). Most zircons with negative Eu anomaly were not included in the diagram because their Ce concentrations are below the detection limit.

The contents of Ti for all zircon types are in a narrow range and rarely exceed tens of ppm. Y and U concentrations range from 457 to 1644 ppm and from 84 to 783 ppm for zircons with oscillatory zoning and on the Y vs U, Y vs Ce/Ce* and Y vs Yb/Sm diagrams (see Fig. 7), most points are within the fields characteristic of zircons from lamproites (Belousova et al., 2002). In opposite, Y is strongly variable in type 2 of recrystallized zircons (138–3784 ppm). Recrystallized zircons of type 1 with low REEs, predictably shows low level of Y content. Both types of recrystallized zircons predominantly show lower U

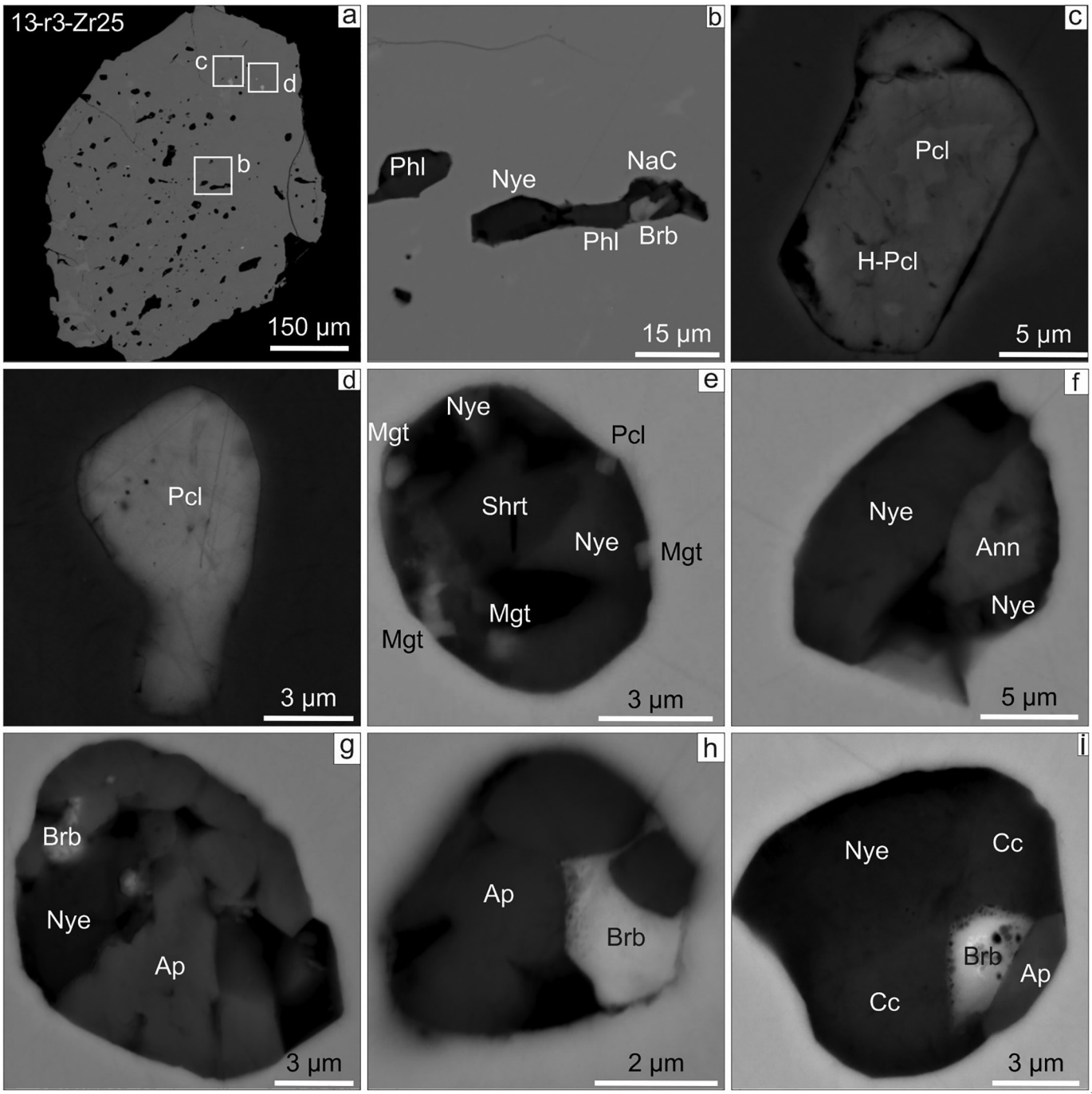

Fig. 4. Secondary multiphase inclusions in zircon from highly weathered damtjernite (depth 13.0 m), BSE images. Phl – F-rich phlogopite (F – up to 3.6 wt%), Ann – F-rich annite; Nye – nyerereite (?), Shrt – shortite; Brb – burbankite-khanneshite, NaC – Na-rich hydrated carbonate, Pcl – fluorcalciopyrochlore, H-Pcl – hydropyrochlore, Ap – fluorapatite, Cc – calcite. Elemental maps and Raman data for the inclusions B and I see Fig. S5 and S6.

contents compared to zircons with oscillatory zoning (see Fig. 7). Zircons with oscillatory zoning and recrystallized zircons of type 2 show strong variation in Th (22–4560 ppm). Contrary, recrystallized zircons of type 1 have much lower Th concentrations (1.4–20 ppm). Nb contents range from 4 to 32 ppm in zircons with oscillatory zoning, and Ta are generally low (up to 2 ppm). The most significant variations of Nb are in recrystallized zircons of type 2 (6–192 ppm), but their Ta contents are similar to zircons with oscillatory zoning. Recrystallized zircons of type 1 show lower concentrations of Nb and Ta. Nb/Ta ratios in zircons are variable, but reach almost 4600, such high Nb/Ta values are a result of the unusually low concentrations of Ta in zircons (see Fig. 7). These Nb/Ta values are higher than those for this mineral from lamproites and carbonatites (Belousova et al., 2002). However, high Nb/Ta are typical in zircons from some carbonatite complex (Doroshkevich et al., 2017, 2018; Tichomirowa et al., 2013). Such a relationship can reflect Nb enrichment of the carbonatite complexes.

4.4. Hf isotopic compositions

The Hf-isotope data for the zircons are reported in Supplementary Table S6 and are displayed in Fig. 8. The measured $^{176}Hf/^{177}Hf$ ratios of the two studied zircon grains (r1-160.7-1 and r1-24.6-2) that were

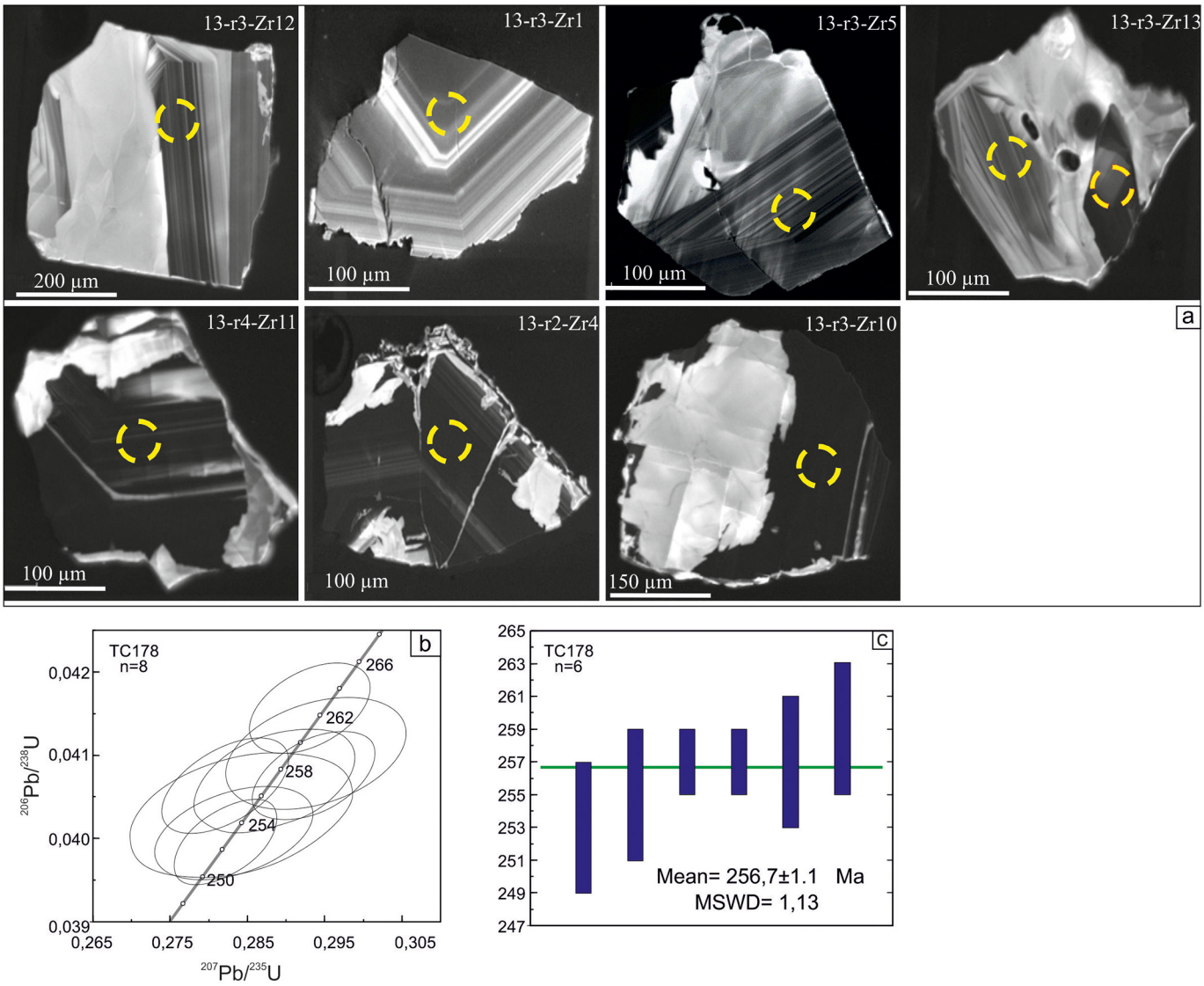

Fig. 5. CL images of zircons, U-Pb concordia diagram and weighted mean age for the zircons with oscillatory zoning from the highly weathered damtjernite (depth 13.0 m).

contaminated by multiphase inclusions (see trace element section) show values of 0.282015 and 0.282250, which correspond to an extremely low εHf (T) values of (−21.5) and (−13.9), respectively. Both analyses were excluded from discussion of Hf isotopic compositions. Measured $^{176}Lu/^{177}Hf$ ratios are >0.0043 in both oscillatory zoned and recrystallized zircon types, nevertheless the recrystallized zircons of type 1 show the lower $^{176}Lu/^{177}Hf$ (Fig. 8a). The $^{176}Hf/^{177}Hf$ ratios of the zircons vary from 0.282602 to 0.282793. There is no particular difference between $^{176}Hf/^{177}Hf$ isotope ratios for oscillatory zoned and recrystallized zircons. For example, the grain r3-13-12 represents the oscillatory zoned type and has $^{176}Hf/^{177}Hf = 0.2822666$, whereas in the recrystallized part of this grain, described as type 2 of recrystallized zircons, $^{176}Hf/^{177}Hf = 0.2822662$.

The broad ranges in Hf-isotope compositions are reflected in their εHf values of (−0.6) – (+6.3) that were calculated assuming an age of 256 Ma. Fig. 8b shows a plot of the εHf (T) vs. age (Ma) for the Chuktukon zircons. It also includes εHf (T) isotope compositions for the zircons of the Triassic Siberian kimberlites (Agashev et al., 2020; Sun et al., 2018) and the ultramafic–mafic Noril'sk-1 intrusion (Malitch et al., 2013), alkaline rocks of the Maymecha-Kotuy area and Guli complex (Carlson et al., 2006; Ghobadi et al., 2018; Malitch et al., 2018). On this plot, the Chuktukon samples display larger Hf-isotope variations, partially overlapping with the field of ultramafic–mafic Noril'sk-1 intrusion and alkaline rocks of the Maymecha- Kotuy area and Guli complex, whereas the zircons of the Triassic Siberian kimberlites have more radiogenic Hf-isotope values.

5. Discussion

5.1. Interpretation of zircon U-Pb age data

The new U-Pb age determination (256.7 ± 1.1 Ma) reported here for a damtjernite is in good agreement with previous U-Pb perovskite age result (252 ± 12 Ma) (Chebotarev et al., 2017a). On the other hand, the previously obtained Ar-Ar rippite (231 ± 2.7 Ma; Chebotarev et al., 2017a), Ar-Ar and Rb-Sr mica (243 ± 3 and 241 ± 1 Ma; Nosova et al., 2020) ages for the Chadobets rocks are younger than our new U-Pb zircon and previously obtained U-Pb perovskite age results (Chebotarev et al., 2017a). The Argon system stability of rippite at different PT-parameters has not been studied. It is possible that younger Ar-Ar ages are related to resetting of argon system, as Ar can be easily lost from minerals, and the age may correspond to a widely distributed and intense late hydrothermal event at Chadobets. Rb-Sr appears to be

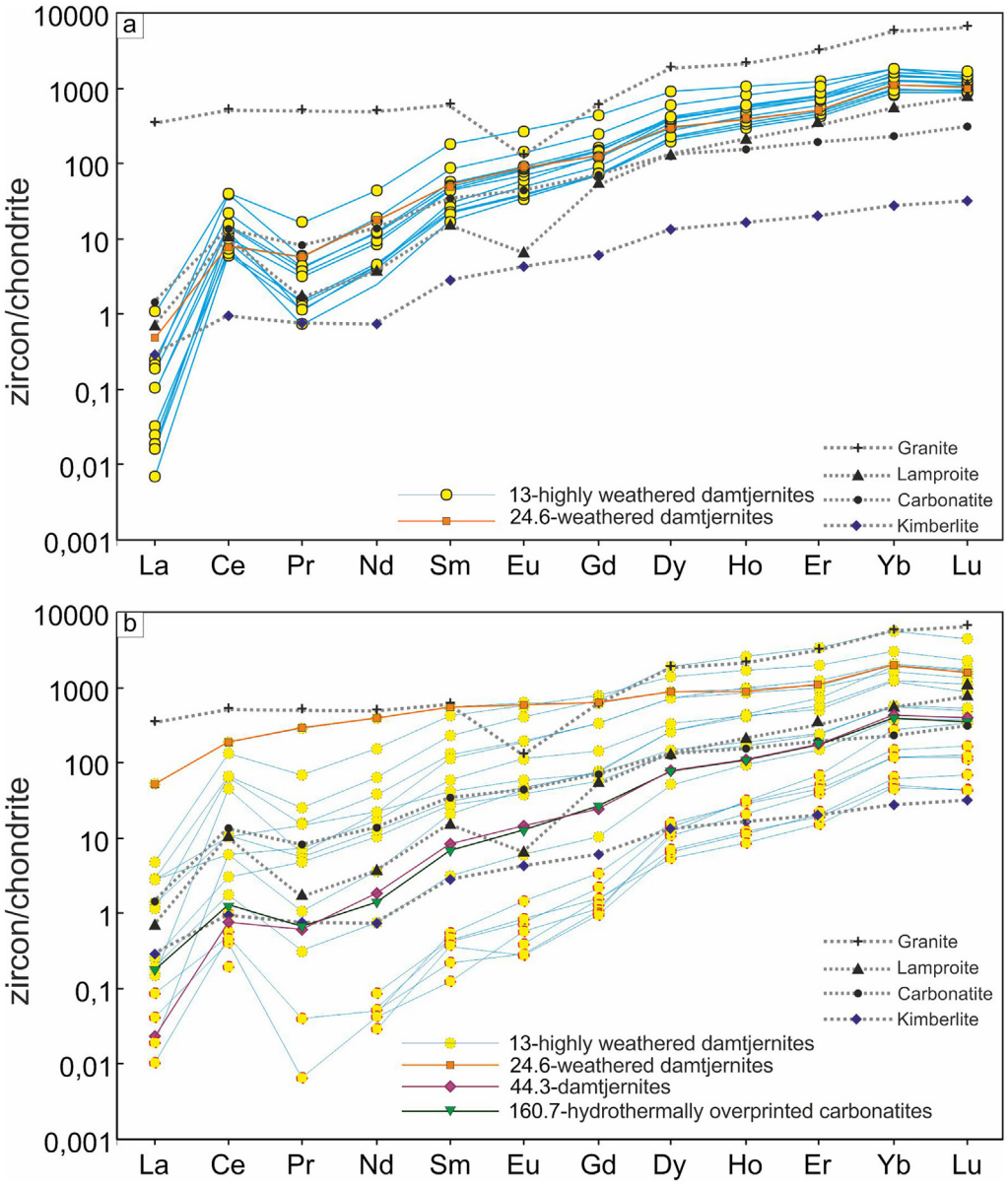

Fig. 6. Chondrite-normalized REE plot of zircons with (a) oscillatory zoning and (b) type 1 (dash red lines) and type 2 (dash black lines) recrystallized zircons from the Chuktukon complex. Patterns for zircons from kimberlites, carbonatites, lamproites and granites after Belousova et al. (2002). Chondrite- and primitive-mantle normalizing values are from Sun and McDonough (1989). (For interpretation of the references to colour in this figure legend, the reader is referred to the web version of this article.)

more robust, nevertheless, minerals for Rb-Sr dating need to be carefully evaluated to assess subsequent alteration by secondary processes.

The difference in ages can be explained as a consequence of the use of different dating methods and different closure temperature of used minerals. Timescales of isotope closure vary considerably and depend on a number of parameters. For example, reported Rb-Sr ages are ~23 Ma younger than ages determined U-Pb in zircon for the mantle-derived rocks of Great Dyke in the Zimbabwe Craton that intruded into presumably hot country rock, such that the thermal gradient between the dyke and the ambient country rocks was small (Nebel and Mezger, 2008).

Lapin (2001) and Kirichenko et al. (2012) mentioned basalt xenoliths in damtjernite pipes, but the emplacement age of country basalts is unknown. Nevertheless, Paton et al. (2010) and Ivanov et al. (2013) reported ages of 250 Ma and 255 Ma for the dolerite sills occurring in close proximity (100 and 300 km to the west and to the south) to the Chadobets uplift.

The age data obtained for the Chuktukon rocks are similar to those of the Siberian Large Igneous Province that includes the Permian-Triassic Siberian Trap (252–250 Ma) as well as meimechites and extensive alkaline magmatism involving kimberlites, lamproites, ultramafic lamprophyres and carbonatites (see Fig. 1a) (e.g., Basu et al., 1995; Burgess and Bowring, 2015; Carlson et al., 2006; Dalrymple et al., 1995; Ernst et al., 2018; Ghobadi et al., 2018; Ivanov et al., 2013; Kogarko and Zartman, 2011; Letnikova et al., 2014; Malitch et al., 2015; Sun et al., 2014; Vrublevskii et al., 2005), therefore suggesting a temporal relation to the Siberian superplume activity.

5.2. Interpretation of inclusions in zircon

The present study of inclusions in the Chuktukon zircons provides evidence for different sources of this mineral. Zircons from carbonatite strongly show carbonatite affinity, whereas zircons from damtjernites indicate two possible sources: alkaline silicate and carbonate. In general,

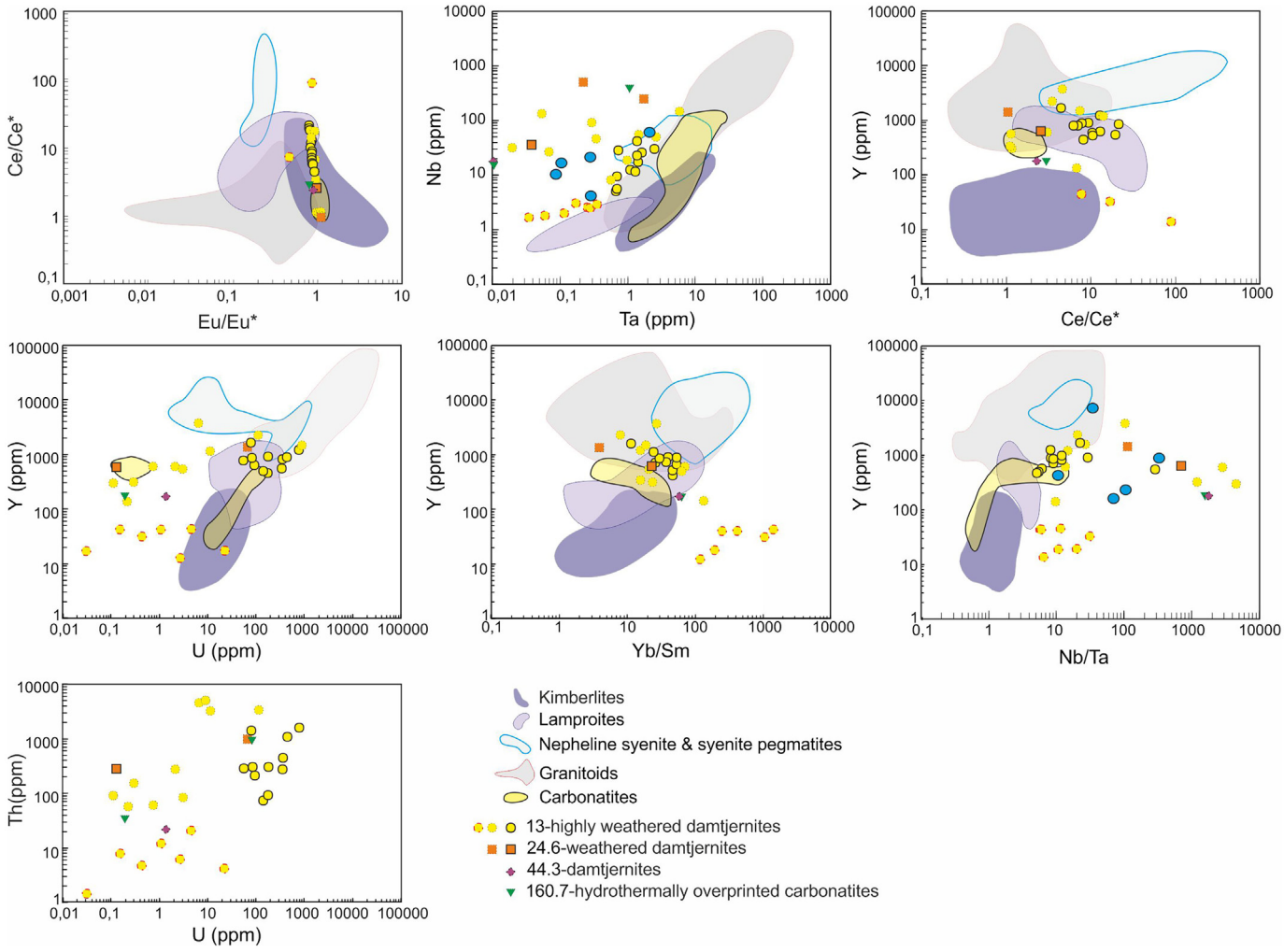

Fig. 7. Trace-element compositions of zircons with oscillatory zoning (bold lines) and type 1 (dash red lines) and type 2 (dash black lines) recrystallized zircons from the Chuktukon complex. Fields for zircons derived from different rock types are from Belousova et al. (2002). Also shown are data (blue circles) for zircons from some carbonatite complex (Doroshkevich et al., 2017, 2018). (For interpretation of the references to colour in this figure legend, the reader is referred to the web version of this article.)

mineral composition of inclusions (calcite, dolomite, fluorapatite, mica, Na-amphibole) in the zircons of the Chuktukon damtjernites is quite similar to that of inclusions hosted by olivine of the neighboring Terina aillikites (Prokopyev et al., 2020). It should be noted that nyererite (or nyerereite-like phase), burbankite-khanneshite and shortite are common phases in carbonate-rich inclusions in zircon. Ba-Sr-REE-Ca-carbonates (burbankite-khanneshite, strontianite, etc.) are ordinary accessory phases in the Chuktukon calciocarbonatites (Chebotarev

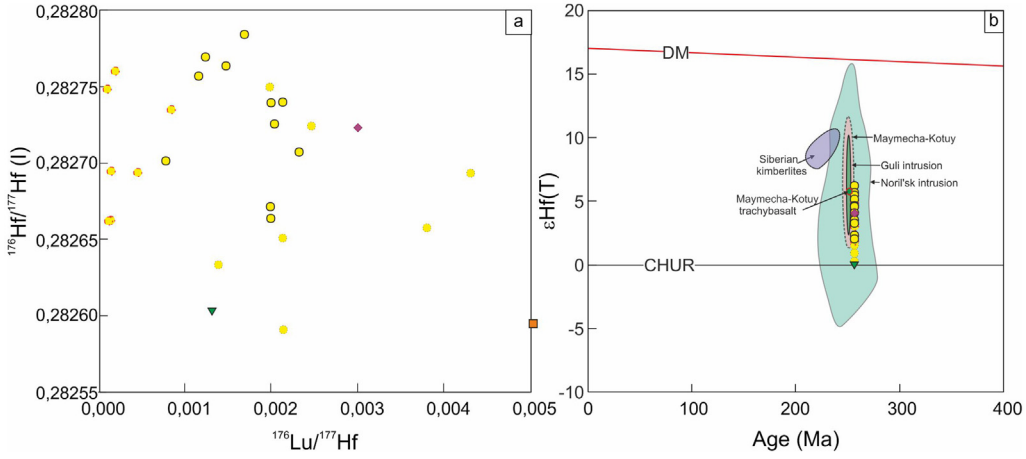

Fig. 8. (a) $^{176}Hf/^{177}Hf$ (I) vs $^{176}Lu/^{177}Hf$(I) plot for the Chuktukon zircons; (b) Initial Hf isotopic compositions of the Chuktukon zircons plotted over the time of damtjernite emplacement Also shown are data for the alkaline rocks of the Maymecha-Kotuy area and Guli rocks (Carlson et al., 2006; Ghobadi et al., 2018; Malitch et al., 2018), the Triassic Siberian kimberlites (Agashev et al., 2020; Sun et al., 2018) and the ultramafic–mafic Noril'sk-1 intrusion (Malitch et al., 2013). Symbols are as Fig. 7.

et al., 2017a, 2017b; Doroshkevich et al., 2019; Sharygin et al., 2016a, 2016b), but previously we did not find Na-Ca-carbonates in these rocks. However, alkali-rich carbonates (nyerereite, shortite, eitelite, bradleyite, northupite, burbankite and others) are omnipresent in multiphase mineral-hosted inclusions from carbonatites, phoscorites and silicate rocks of many intrusive alkaline ultramafic complexes around the world: Guli and Krestovskiy, Polar Siberia, Russia (Kogarko and Zartman, 2011; Panina, 2005); Gardiner, Greenland (Nielsen et al., 1997; Veksler et al., 1998); Belaya Zima and Bol'shaya Tagna, Eastern Sayan, Russia (Andreeva, 2014; Andreeva et al., 2004, 2006, 2007; Sharygin and Doroshkevich, 2017); Kovdor, Afrikanda and other complexes, Kola, Russia (Potter et al., 2020; Veksler et al., 1998); Phalaborwa complex, South Africa (Sharygin et al., 2011); Oka, Canada (Chen et al., 2013; see also review by Chakhmouradian et al., 2016). In general, the phase compositions of multiphase inclusions in zircons (presence of nyerereite and shortite) may reflect the presence of Na-rich carbonatite melt in the Chuktukon complex similar to the natrocarbonatite lava of the Oldonyo Lengai volcano in Tanzania (Sharygin et al., 2012).

5.3. Interpretation of trace-element and Hf-isotope data

The Chuktukon zircon grains have complex internal morphology and typically show a complex structure on CL images with preservation of primary zoning and new zircon overgrowths and recrystallization (type 1 and 2). Zircon grains with oscillatory zoning are typical of mineral grown from a melt. In addition, these zircons have REE patterns with a steep increase in relation to HREE concentrations typical for igneous zircons (see Fig. 6). In geochemical discriminant diagrams (see Fig. 7), these zircon grains plot in the field of lamproitic zircons. A lack of negative Eu anomaly is consistent with the absence of Eu anomaly in the Chuktukon aillikite-damtjernite host rocks (Doroshkevich et al., 2019). Recrystallization type 2 and new zircon overgrowths can be attributed to interaction with a carbonatite melt. This interaction resulted in formation of zircons with higher concentrations of REEs and Nb, without changes for $^{176}Lu/^{177}Hf$ and $^{176}Hf/^{177}Hf$ ratios. The carbonatite melt is proposed to be the carrier of REE and Nb, and as the reprecipitation process brought these elements into zircon. Such process (infiltration of carbonatite melt) is responsible for the appearance of secondary multiphase inclusions in zircons with mineral association typical of carbonatites (alkali-rich carbonates, fluorcalciopyrochlore, fluorapatite, Ba-Sr-REE-Ca-carbonates, calcite, dolomite, phlogopite and others) and zircon recrystallization. Similarly, carbonatite melts that caused recrystallization of zircon grains were reported from several carbonatite massifs (e.g. Tichomirowa et al., 2013).

Type 1 recrystallized zircons are Nb- Th- U- Y- and REE-poor. This suggests dissolution of igneous zircon and reprecipitation of trace-element-poor zircon, possibly from late-stage melt or fluid, which were depleted in these trace elements as a result of their accumulation in other competing accessory mineral phases. The interaction with such a melt/fluid led to decreasing in $^{176}Lu/^{177}Hf$, while $^{176}Hf/^{177}Hf$ ratios did not change. These features are typical for a recrystallization process of zircon in the presence of an aqueous fluid (e.g., Chen et al., 2010; Tichomirowa et al., 2013). In addition, this type of zircons shows negative Eu anomaly that is consistent with the K-feldspar crystallization in the Chuktukon damtjernites and carbonatites (see petrographic description, Doroshkevich et al., 2019). However, $^{176}Hf/^{177}Hf$ ratios in the recrystallized zircons of type 1 are similar to those of magmatic zircons and zircons of type 2 recrystallization. This indicates that Hf isotopic compositions of recrystallized zircons record the signature of their primary magma source.

5.4. Magma source characteristic

The Sr-Nd isotopic compositions of the Chadobets alkaline silicate rocks and carbonatites suggest that their primary magmas were derived from a common moderately depleted mantle source: $^{87}Sr/^{86}Sr(I)$ from 0.7024 to 0.7043 and εNd(T) from 4.09 to 5.08 (Doroshkevich et al., 2019; Nosova et al., 2020). On the other hand, zircons from the Chuktukon rocks have variable Hf isotopic composition implying complex evolution history of their source(s).

Broad Hf-isotope variations in zircons from alkaline carbonatite complexes and kimberlites have been documented previously (e.g. Griffin et al., 2000; Nedosekova et al., 2013, 2015, 2018; Tichomirowa et al., 2013; Wu et al., 2011), suggesting that the parental melt was contaminated by crustal material or more than one source was involved in generating the parental melts. Crustal contamination for the Chuktukon rocks can be ruled out given the Pb isotopic data ($^{206}Pb/^{204}Pb$ = 18.4–19.0, $^{208}Pb/^{204}Pb$ = 38.3–38.8, $^{207}Pb/^{204}Pb$ = 15.5–15.6) and high Ce/Pb and Nb/U ratios (6–35 and 34–434, respectively) of the Chadobets aillikites-damtjernites (Doroshkevich et al., 2019; Nosova et al., 2020). Furthermore, similar Hf-isotope compositions of magmatic and recrystallized zircons indicates that the minerals record the signature of their primary magma source. Therefore, we propose that the Hf isotopic data obtained here represent those of the primary magma, indicating that the source region of the Chuktukon rocks contained the moderately depleted mantle component (with εHf ~6) and component with εHf ~0. The last component can be material of subcontinental lithospheric source (with εNd and εHf ~0) as proposed by Griffin et al. (2000). Subcontinental lithospheric mantle component in the source has been reported previously for the ultramafic–mafic Noril'sk-1 intrusion (Malitch et al., 2013) and Siberian kimberlites (e.g. Griffin et al., 2000; Howarth et al., 2014). On the other side, Sharma et al. (1991, 1992) suggested that geochemical characteristics of the Permian-Triassic Putorana basalts with fairly homogeneous Sr-Nd isotope compositions (εNd = 0 to +2.5, $^{87}Sr/^{86}Sr$ = 0.7046 to 0.7052) are characteristics of the superplume material and comprised about 90–95% of the Siberian superplume. In addition, the rocks of the Maimecha-Kotuy Province, including Guli complex, which show similar Sr-Nd-Hf isotopic composition and trace element characteristics to that of at Chadobets, are regarded as the products of the Siberian superplume (Carlson et al., 2006; Ghobadi et al., 2018; Ryabchikov et al., 2009; Sobolev et al., 2009).

Some authors (Kogarko and Ryabchikov, 2000; Ryabchikov et al., 2009) suggested that the primary meimechite magmas of the Maimecha-Kotuy rocks were produced by an interaction of partial melted fertile lherzolite with the lithosphere mantle material (harzburgite) during Siberian superplume activity. Sobolev et al. (2009) proposed that the metasomatic agent was silicate-carbonate melt released from recycled oceanic crust of the plume head.

Recent studies (Doroshkevich et al., 2019; Nosova et al., 2018, 2020) show that the source region of the Chadobets rocks had a two stage temporal evolution of the metasomatic processes in the subcontinental lithospheric mantle beneath the southern part of Siberian craton. Nosova et al. (2018, 2020) demonstrated that phlogopite-rich metasomatites were the first metasomatic component in the mantle prior to the Siberian plume activity. This is based on olivine trace-element data and Sr-Nd-Pb isotopic composition of the Devonian Ilbokich aillikite-damtjernite complex occurring in close proximity to the Chadobets complex. The authors concluded that metasomatism was related to incorporation of subducted material in the source during the Caledonian collision at southern boundary of the Siberian craton (Nosova et al., 2020). The Triassic aillikite-damtjernite series and carbonatites of the Chadobets complex characterise the following stage and are interpreted to represent a carbonate mantle metasomatism (Doroshkevich et al., 2019; Nosova et al., 2018, 2020). Multiphase inclusions and geochemical features in the Chuktukon zircons (see Figs. 6 and 7) affirm the (per)alkaline ultramafic and carbonatite characteristics of their parental melts and support an imprint of the carbonate component in their mantle source. In our opinion, trace-element enriched metasomatic melts/fluids of carbonatitic affinity was produced by the Siberian superplume activity.

6. Conclusions

The new U-Pb, Hf-isotope and trace-elements data collected during this study in combination with petrography of zircon-hosted inclusions from the Chuktukon complex lead to the following conclusions:

The oscillatory zoned zircons from the Chuktukon damtjernites yield U-Pb age of 256.7 ± 1.1 Ma. This age is in a good agreement with the Permian-Triassic Siberian Trap event as well as meimechites and extensive alkaline magmatism involving kimberlites, lamproites, ultramafic lamprophyres and carbonatites of the Siberian craton.

Oscillatory zoned zircon domains, which preserved primary isotope signatures, show evidence for recrystallization processes caused by infiltration of carbonatite melt and late stage fluid. These interactions resulted in formation of zircons with variable concentrations of REEs, Th, U and Nb, but unchanged $^{176}Hf/^{177}Hf$ ratios. Such recrystallization was accompanied by formation of multiphase inclusions of carbonatite affinity.

Source region of the Chuktukon rocks was heterogeneous, and characterized by the presence of moderately depleted mantle component (with εHf ~6) and less radiogenic Hf isotope endmember (with εHf ~0).

Declaration of Competing Interest

The authors declare that they have no known competing financial interests or personal relationships that could have appeared to influence the work reported in this paper.

Acknowledgements

Investigations of inclusions were done on state assignment of IGM SB RAS (0330-2019-0002 and 0330-2016-0005), GIN SB RAS (AAAA-A16-116122110027-2) and the Initiative Project of Ministry of Science and Higher Education of the Russian Federation and by Act 211 of the Government of the Russian Federation, agreement no. 02.A03.21.0006. Geochemical and isotopic studies of the zircons were supported by the Russian Science Foundation (grant 19-77-10004). The authors gratefully thank Prof. Xian-Hua Li for the editorial comments, anonymous reviewers for the insightful reviews, which led to the significant improvement of the manuscript.

Appendix A. Supplementary data

Supplementary data to this article can be found online at https://doi.org/10.1016/j.lithos.2020.105957.

References

Agashev, A.M., Chervyakovskaya, M.V., Serov, I.V., Tolstov, A.V., Agasheva, E.V., Votyakov, S.L., 2020. Source rejuvenation vs. re-heating: constraints on Siberian kimberlite origin from U-Pb and Lu-Hf isotope compositions and geochemistry of mantle zircons. Lithos 364–365, 1–10.

Andersen, T., 2002. Correction of common Pb in U–Pb analyses that do not report ^{204}Pb. Chem. Geol. 192, 59–79.

Andreeva, I.A., 2014. Carbonatitic melts in olivine and magnetite from rare metal carbonatite of the Belaya Zima alkaline carbonatite complex (East Sayan, Russia). Dokl. Earth Sci. 455 (2), 436–440.

Andreeva, I.A., Kovalenko, V.I., Kononkova, N.N., 2004. Chemical composition of magma (melt inclusions) of melilite-bearing nephelinite from the Belaya Zima carbonatite complex, Eastern Sayan. Dokl. Earth Sci. 394 (1), 116–119.

Andreeva, I.A., Kovalenko, V.I., Kononkova, N.N., 2006. Natrocarbonatitic melts of the Bol'shaya Tagna Massif, the Eastern Sayan Region. Dokl. Earth Sci. 408 (4), 542–546.

Andreeva, I.A., Kovalenko, V.I., Nikiforov, A.V., Kononkova, N.N., 2007. Compositions of magmas, formation conditions, and genesis of carbonate-bearing ijolites and carbonatites of the Belaya Zima alkaline carbonatite complex, Eastern Sayan. Petrology 15 (6), 551–574.

Arndt, N., Chauvel, C., Czamanske, G., Fedorenko, V., 1998. Two mantle sources, two plumbing systems: tholeiitic and alkaline magmatism of the Maymecha River basin, Siberian flood volcanic province. Contrib. Mineral. Petrol. 133, 297–313. https://doi.org/10.1007/s004100050453.

Basu, A.R., Poreda, R.J., Renne, P.R., Telchmann, F., Vasiliev, Y.R., Sobolev, N.V., Turrin, B.D., 1995. High-3He plume origin and temporal–spatial evolution of the Siberian flood basalts. Science 269 (5225), 825–882. https://doi.org/10.1126/science.269.5225.822.

Belousova, E.A., Walters, S., Griffin, W.L., O'Reilly, S.Y., Fisher, N.I., 2002. Igneous zircon: trace element composition as an indicator of source rock type. Contrib. Mineral. Petrol. 143, 602–622.

Black, L.P., Kamo, S.L., Allen, C.M., 2003. TEMORA 1: a new zircon standard for Phanerozoic U–Pb geochronology. Chem. Geol. 200, 155–170.

Bouvier, A., Vervoort, J.D., Patchett, P.J., 2008. The Lu-Hf and Sm-Nd isotopic composition of CHUR: constraints from unequilibrated chondrites and implications for the bulk composition of terrestrial planets. Earth Planet. Sci. Lett. 273, 48–57.

Burgess, S.D., Bowring, S.A., 2015. High-precision geochronology confirms voluminous magmatism before, during, and after Earth's most severe extinction. Sci. Adv. 1 (7), e1500470. https://doi.org/10.1126/sciadv.1500470.

Carlson, R.W., Czamanske, G., Fedorenko, V., Ilupin, I., 2006. A comparison of Siberian meimechites and kimberlites: implications for the source of high-Mg alkali magmas and flood basalts. Geochem. Geophys. Geosyst. 7 (11). https://doi.org/10.1029/2006GC001342.

Chakhmouradian, A.R., Reguir, E.P., Zaitsev, A.N., 2016. Calcite and dolomite in intrusive carbonatites. I. Textural variations. Mineral. Petrol. 110, 333–360.

Chebotarev, D.A., Doroshkevich, A.G., Sharygin, V.V., Yudin, D.S., Ponomarchuk, A.V., Sergeev, S.A., 2017a. Geochronology of the Chuktukon carbonatite massif, Chadobets uplift (Krasnoyarsk Territory). Russ. Geol. Geophys. 58, 1222–1231.

Chebotarev, D.A., Doroshkevich, A.G., Klemd, R., Karmanov, N.S., 2017b. Evolution of Nb mineralization in the Chuktukon carbonatite massif, Chadobets uplift (Krasnoyarsk Territory, Russia). Period. Mineral. 86, 99–118. https://doi.org/10.2451/2017PM733.

Chen, R.-X., Zheng, Y.-F., Xie, L., 2010. Metamorphic growth and recrystallization of zircon: distinction by simultaneous in-situ analyses of trace elements, U–Th–Pb and Lu–Hf isotopes in zircons from eclogite-facies rocks in the Sulu orogen. Lithos 114, 132–154.

Chen, W., Kamenetsky, V.S., Simonetti, A., 2013. Evidence for the alkaline nature of parental carbonatite melts at Oka complex in Canada. Nat. Commun. 4, 2687.

Dalrymple, G.B., Czamanske, G.K., Fedorenko, V.A., Simonov, O.N., Lanphere, M.A., Likhachev, A.P., 1995. A reconnaissance 40Ar/39Ar geochronologic study of ore-bearing and related rocks, Siberian Russia. Geochim. Cosmochim. Acta 59 (10), 2071–2083. https://doi.org/10.1016/0016-7037.

Dashkevich, N.N., 1999. Regional prediction of kimberlite magmatism in the southwestern Siberian Platform. Geologiya i poleznye iskopaemye Krasnoyarskogo kraya (Geology and Mineral Resources of Krasnoyarsk District) in Russian, pp. 31–42.

DeBievre, P., Taylor, P.D.P., 1993. Table of the isotopic composition of the elements. Int. J. Mass Spectrom. Ion Process. 123, 149.

Doroshkevich, A.G., Veksler, I.V., Klemd, R., Khromova, E.A., Izbrodin, I.A., 2017. Trace-element composition of minerals and rocks in the Belaya Zima carbonatite complex (Russia): implications for the mechanisms of magma evolution and carbonatite formation. Lithos 284-285, 91–108.

Doroshkevich, A.G., Prokopyev, I.R., Izokh, A.E., Klemd, R., Ponomarchuk, A.V., Nikolaeva, I.V., Vladykin, N.V., 2018. Isotopic and trace element geochemistry of the Seligdar magnesiocarbonatites (South Yakutia, Russia): insights regarding the mantle evolution beneath the Aldan-Stanovoy shield. J. Asian Earth Sci. 154, 354–368.

Doroshkevich, A.G., Chebotarev, D.A., Sharygin, V.V., Prokopyev, I.R., Nikolenko, A.M., 2019. Petrology of alkaline silicate rocks and carbonatites of the Chuktukon massif, Chadobets uplift, Russia: sources, evolution and relation to the Triassic Siberian LIP. Lithos 332–333, 245–260.

Elhlou, S., Belousova, E.A., Griffin, W.L., Pearson, N.J., O'Reilly, S.Y., 2006. Trace element and isotopic composition of GJ red zircon standard by Laser Ablation. Geochim. Cosmochim. Acta 70 (18), A158.

Ernst, R.E., Davies, D.R., Jowitt, S.M., Campbell, I.H., 2018. When do mantle plumes destroy diamonds? Earth Planet. Sci. Lett. 502, 244–252.

Fedorenko, V., Czamanske, G., Zenko, T., Budahn, J., Siems, D., 2000. Field and geochemical studies of the Melilite-Bearing Arydzhangsky Suite, and an overall perspective on the Siberian Alkaline–Ultramafic Flood-Volcanic Rocks. Int. Geol. Rev. 42, 769–804. https://doi.org/10.1080/00206810009465111.

Ghobadi, M., Gerdes, A., Kogarko, L., Hoefer, H., Brey, G., 2018. In situ LA-ICPMS isotopic and geochronological studies on carbonatites and phoscorites from the Guli Massif, Maymecha-Kotuy, Polar Siberia. Geochem. Int. 56 (8), 766–783. https://doi.org/10.1134/S0016702918080049.

Griffin, W.L., Pearson, N.J., Belousova, E., Jackson, S.E., van Achterbergh, E., O'Reilly, S.Y., Shee, S.R., 2000. The Hf isotope composition of cratonic mantle: LAM-MC-ICPMS analysis of zircon megacrysts in kimberlites. Geochim. Cosmochim. Acta 64, 133–147.

Griffin, W.L., Pearson, N.J., Belousova, E.A., Saeed, A., 2007. Reply to "Comment to short-communication 'Comment: Hf-isotope heterogeneity in zircon 91500' by W.L. Griffin, N.J. Pearson, E.A. Belousova and A. Saeed (Chemical Geology 233 (2006) 358–363)" by F. Corfu. Chem. Geol. 244, 354–356.

Griffin, W.L., Powell, W.J., Pearson, N.J., O'Reilly, S.Y., 2008. GLITTER: data reduction software for laser ablation ICP-MS. In: Sylvester, P. (Ed.), Laser Ablation-ICP-MS in the Earth Sciences: Mineralogical Association of Canada Short Course Series. 40, pp. 204–207 (Appendix 2).

Howarth, G.H., Barry, P.H., Pernet-Fisher, J.F., Baziotis, I.P., Pokhilenko, N.P., Pokhilenko, L.N., Bodnar, R.J., Taylor, L.A., Agashev, A.M., 2014. Superplume metasomatism: evidence from Siberian mantle xenoliths. Lithos 184, 209–224.

Ivanov, A.V., He, H., Yan, L., Ryabov, V.V., Shevko, A.Y., Palesskii, S.V., Nikolaeva, I.V., 2013. Siberian Traps large igneous province: evidence for two food basalt pulses around the Permo–Triassic boundary and in the Middle Triassic, and contemporaneous

granitic magmatism. Earth Sci. Rev. 122, 58–76. https://doi.org/10.1016/j.earscirev.2013.04.001.

Jackson, S.E., Pearson, N.J., Griffin, W.L., Belousova, E.A., 2004. The application of laser ablation microprobe-inductively coupled plasma-mass spectrometry (LAM-ICPMS) to in situ U-Pb zircon geochronology. Chem. Geol. 211, 47–69.

Kargin, A.V., Nosova, A.A., Postnikov, A.V., Chugaev, A.V., Postnikova, O.V., Popova, L.P., Poshibaev, V.V., Sazonova, L.V., Dokuchaev, A.Y., Smirnova, M.D., 2016. Devonian ultramafic lamprophyre in the Irkineeva–Chadobets trough in the southwest of the Siberian Platform: age, composition, and implications for diamond potential prediction. Geol. Ore Depos. 58, 383–403. https://doi.org/10.1134/S1075701516050068.

Kemp, A.I.S., Wormald, R.J., Whitehouse, M.J., Price, R.C., 2005. Hf isotopes in zircon reveal contrasting sources and crystallization histories for alkaline to peralkaline granites of Temora, southeastern Australia. Geology 33, 797–800.

Kirichenko, T., Zuev, K., Perfilova, O.Yu., Sosnovskaya, O., Smokotina, I., Markovich, L.A., Borodin, E., Mironyuk, E., 2012. State Geological Map of Russian Federation, Scale 1: 1000000 (Third Generation). Ser. Angaro-Eniseysk. Sheet O-47 Bratsk. Explanatory Note. Cartografic Factory of VSEGEI, St. Petersburg. pp. 163–179 (In Russian).

Kogarko, L.N., Ryabchikov, I.D., 2000. Geochemical evidence for meimechite magma generation in the subcontinental lithosphere of Polar Siberia. Journal of Asian Earth Sciences 18, 195–203. https://doi.org/10.1016/S1367-9120(99)00041-3.

Kogarko, L.N., Zartman, R.E., 2011. New data on the age of the Guli intrusion and implications for the relationships between alkaline magmatism in the Maymecha–Kotuy province and the Siberian Superplume: U–Th–Pb isotopic systematics. Geochem. Int. 49 (5), 439–448. https://doi.org/10.1134/S0016702911050065.

Lafuente, B., Downs, R.T., Yang, H., Stone, N., 2016. The power of databases: the RRUFF project. In: Armbruster, T., Danisi, R.M. (Eds.), Highlights in Mineralogical Crystallography. W. de Gruyter GmbH, Berlin, Germany, pp. 1–29. https://doi.org/10.1515/9783110417104-003.

Lapin, A.V., 2001. About kimberlites of the Chadobets uplift in connection with a problem of the formational-metallogeny analysis of the platform alkaline ultrabasic magmatic rocks. Otechestvennaya Geol. 4, 30–35 (In Russian).

Lapin, A.V., Lisitzyn, D.V., 2004. About mineralogical typomorphism of alkaline ultrabasic magmatic rocks of Chadobets uplift. Otechestvennaya Geol. 683, 93 (In Russian).

Letnikova, E.F., Izokh, A.E., Nikolenko, E.I., Pokhilenko, N.P., Shelestov, V.O., Geng, Hilen, Lobanov, S.S., 2014. Late Triassic high-potassium trachytic volcanism of the northeast of the Siberian platform: evidence in the sedimentary record. Doklady Earth Sci. 459 (1), 1344–1347. https://doi.org/10.1134/S1028334X14110221.

Lightfoot, P.C., Hawkesworth, C.J., Hergt, J., Naldrett, A.J., Gorbachev, N.S., Fedorenko, V.A., Doherty, W., 1993. Remobilization of the continental lithosphere by a mantle plume: major-, trace-element, and Sr-, Nd- and Pb-isotopic evidence frompicritic and tholeiitic lavas of the Noril'sk district, Siberia. Contrib. Mineral. Petrol. 114, 171–188. https://doi.org/10.1007/BF00307754.

Lomayev, V.G., Serdyuk, S.S., 2011. The Chuktukon Nb-TR deposit - the priority object for modernization of the Russian rare-earth industry. J. Siber. Feder. Univ. 4, 132–154.

Malitch, K.N., Belousova, E.A., Griffin, W.L., Badanina, I.Yu., 2013. Hafnium-neodymium constraints on source heterogeneity of the economic ultramafic-mafic Noril'sk-1 intrusion (Russia). Lithos 164–167, 36–46.

Malitch, K.N., Khiller, V.V., Badanina, I.Yu., Belousova, E.A., 2015. Results of dating of thorianite and baddeleyite from carbonatites of the Guli massif. Russian Doklady Earth Sci. 464 (2), 1029–1032.

Malitch, K.N., Kogarko, L.N., Badanina, I.Y., Belousova, E.A., 2018. Hafnium–Neodymium isotope systematics of carbonatites from the Guli Massif (Maimecha–Kotui Province, Russia). Dokl. Earth Sci. 480, 652–655.

Nebel, O., Mezger, K., 2008. Timing of thermal stabilization of the Zimbabwe Craton deduced from high-precision Rb–Sr chronology, Great Dyke. Precambrian Res. 164 (3–4), 227–232.

Nedosekova, I.L., Belousova, E.A., Sharygin, V.V., Belyatsky, B.V., Bayanova, T.B., 2013. Origin and evolution of the Ilmeny-Vishnevogorsky carbonatites (Urals, Russia): insights from trace-elements compositions, Rb-Sr, Sm-Nd, U-Pb, Lu-Hf isotope data. Mineral. Petrol. 107 (1), 101–123. https://doi.org/10.1007/s00710-012-0223-9.

Nedosekova, I.L., Belousova, E.A., Belyatsky, B.V., 2015. Hf isotopes and trace elements as indicators of zircon genesis in the evolution of the alkaline–carbonatite magmatic system (Il'meno–Vishnevogorskii Complex, Urals, Russia). Dokl. Earth Sci. 461 (2), 384–389.

Nedosekova, I.L., Koroteev, V.A., Belyatsky, B.V., Sharygin, V.V., Lepekhina, E.N., Pribavkin, S.V., 2018. U-Pb Dating of niobium ore minerals of the pyrochlore group (Ilmeno-Vishnevogorsk Carbonatite-Miaskite Complex, South Urals). Lithosphere 18 (5), 758–773. https://doi.org/10.24930/1681-9004-2018-18-5-758-773.

Nielsen, T.F.D., Solovova, I.P., Veksler, I.V., 1997. Parental melts of melilitolite and origin of alkaline carbonatite: evidence from crystallized melt inclusions, Gardiner complex. Contrib. Mineral. Petrol. 126, 331–344.

Nosova, A.A., Sazonova, L.V., Kargin, A.V., Smirnova, M.D., Lapin, A.V., Shcherbakov, V.D., 2018. Olivine in ultramafic lamprophyres: Chemistry, crystallisation, and melt sources of Siberian Pre- and post-trap aillikites. Contrib. Mineral. Petrol. 173, 55. https://doi.org/10.1007/s00410-018-1480-3.

Nosova, A.A., Kargin, A.V., Sazonova, L.V., Dubinina, E.O., Chugaev, A.V., Lebedeva, N.M., Yudin, D.S., Larionova, Y.O., Abersteiner, A., Gareev, B.I., 2020. Sr-Nd-Pb isotopic systematic and geochronology of ultramafic alkaline magmatism of the southwestern margin of the Siberian Craton: metasomatism of the sub-continental lithospheric mantle related to subduction and plume events. Lithos, 364–365 https://doi.org/10.1016/j.lithos.2020.105509.

Panina, L.I., 2005. Multiphase carbonate–salt immiscibility in carbonatite melts: data on melt inclusions from the Krestovskiy massif minerals (Polar Siberia). Contrib. Mineral. Petrol. 150, 19–36.

Paton, M.T., Ivanov, A.V., Fiorentini, M.L., McNaughton, M.J., Mudrovska, I., Reznitskii, L.Z., Demonterova, E.I., 2010. Late Permian and Early Triassic magmatic pulses in the Angara-Taseeva syncline, Southern Siberian Traps and their possible influence on the environment. Russ. Geol. Geophys. 51, 1012–1020.

Pearson, N.J., Griffin, W.L., O'Reilly, S.Y., 2008. Mass fractionation correction in laser ablation-multiple collector ICP-MS: implications for overlap corrections and precise and accurate in situ isotope ratio measurement. In: Sylvester, P. (Ed.), Laser-Ablation-ICP-MS in the Earth Sciences : Current Practices and Outstanding. Mineralogical Association of Canada Short Course 40, Vancouver, B.C, pp. 93–116.

Pernet-Fisher, J.F., Howarth, G.H., Pearson, D.G., Woodland, S., Barry, P.H., Pokhilenko, N.P., Agashev, A.M., Taylor, L.A., 2015. Plume impingement on the Siberian SCLM: evidence from Re-Os isotope systematics. Lithos 218–219, 141–154.

Potter, N.J., Kamenetsky, V.S., Chakhmouradian, A.R., Kamenetsky, M.B., Goemann, K., Rodemann, T., 2020. Polymineralic inclusions in oxide minerals of the Afrikanda alkaline-ultramafc complex: implications for the evolution of perovskite mineralisation. Contrib. Mineral. Petrol. 175, 18. https://doi.org/10.1007/s00410-020-1654-7.

Prokopyev, I., Starikova, A., Doroshkevich, A., Nugumanova, Y., Potapov, V., 2020. Petrogenesis of Ultramafic Lamprophyres from the Terina Complex (Chadobets Uplift, Russia): mineralogy and melt inclusion composition. Minerals 10, 419. https://doi.org/10.3390/min10050419.

Rao, N.V.C., Lehmann, B., 2011. Kimberlites, flood basalts and mantle plumes: new insights from the Deccan Large Igneous Province. Earth Sci. Rev. 107, 315–324.

Ryabchikov, I.D., Kogarko, L.N., Solovova, I.P., 2009. Physicochemical conditions of magma formation at the base of the Siberian plume: insight from the investigation of melt inclusions in the meymechites and alkali picrites of the Maimecha—Kotui Province. Petrology 17, 287–299. https://doi.org/10.1134/S0869591109030059.

Scherer, E., Munker, C., Mezger, K., 2001. Calibration of the lutetium–hafnium clock. Science 293, 683–687.

Sharma, M., Basu, A.R., Nesterenko, G.V., 1991. Nd-Sr isotopes, petrochemistry, and origin of the Siberian flood basalts, USSR. Geochim. Cosmochim. Acta 53, 1183–1192. https://doi.org/10.1016/0016-7037(91)90177-7.

Sharma, M., Basu, A.R., Nesterenko, G.V., 1992. Temporal Sr-, Nd-, and Pb-isotopic variations in the Siberian flood basalts: implications for the plume-source characteristics. Earth Planet. Sci. Lett. 113, 365–381. https://doi.org/10.1016/0012-821X(92)90139-M.

Sharygin, V.V., 2017. Tainiolite from Chuktukon carbonatite massif, Chadobets Uplift, Russia. In: Zaitsev, V.A., Ermolaeva, V.N. (Eds.), Proceedings of XXXIV International Conference. "Magmatism of the Earth and Related Strategic Metal Deposits". GEOKHI RAS, pp. 242–244.

Sharygin, V.V., Doroshkevich, A.G., 2017. Mineralogy of secondary olivine-hosted inclusions in calcite carbonatites of the Belaya Zima alkaline massif, Eastern Sayan, Russia: evidence for late-magmatic Na-Ca-rich carbonate composition. J. Geol. Soc. India 90 (11), 524–530.

Sharygin, V.V., Zhitova, L.M., Nigmatullina, E.N., 2011. Fairchildite $K_2Ca(CO_3)_2$ in phoscorites from Phalaborwa, South Africa: first occurrence in alkaline carbonatite complexes. Russ. Geol. Geophys. 52, 208–219. https://doi.org/10.1016/j.rgg.2010.12.015.

Sharygin, V.V., Kamenetsky, V.S., Zaitsev, A.N., Kamenetsky, M.B., 2012. Silicate-natrocarbonatite liquid immiscibility in 1917 eruption combeite-wollastonite nephelinite, Oldoinyo Lengai volcano, Tanzania: melt inclusion study. Lithos 152, 23–39. https://doi.org/10.1016/j.lithos.2012.01.021.

Sharygin, V.V., Doroshkevich, A.G., Chebotarev, D.A., 2016a. Na-Sr-Ba-REE-carbonates and phosphates in carbonatite minerals of Chuktukon massif, Krasnoyarsk territory. Abstract volume of 17th Russian Conference on Fluid Inclusion Studies, Ulan-Ude, GI SB RAS, pp. 180–182 (in Russian).

Sharygin, V.V., Doroshkevich, A.G., Seryotkin, Y.V., Karmanov, N.S., Belogub, E.V., Moroz, T.N., 2016b. A new K-Nb-cyclosilicate $K_2(Nb,Ti)_2(Si_4O_{12})O(O,F)$ from Chuktukon carbonatite massif, Chadobets uplift, Russia. Abstract volume of 2nd European Mineralogical Conference, Rimini, Italy (421–421).

Sobolev, A.V., Sobolev, S.V., Kuzmin, D.V., 2009. Siberian meimechites: origin and relation to flood basalts and kimberlites. Russian Geol. Geophys. 50, 999–1033. https://doi.org/10.1016/j.rgg.2009.11.002.

Stacey, J.S., Kramers, J.D., 1975. Approximation of terrestrial lead isotope evolution by a two-stage model. Earth Planet. Sci. Lett. 26, 207–221.

Staroseltsev, V.S., 2009. Identifying paleorifts as promising tectonic elements for active oil and gas generation. Russ. Geol. Geophys. 50 (4), 358–364.

Sun, S.-S., McDonough, W.F., 1989. Chemical and isotopic systematics of oceanic basalts: implications for mantle composition and processes. Geol. Soc. Lond. Spec. Publ. 42, 313–345. https://doi.org/10.1144/GSL.SP.1989.042.01.19.

Sun, J., Liu, C., Tappe, S., Kostrovitsky, S.I., Wu, F.-Y., Yakovlev, D., Yang, Y.-H., Yang, J.-H., 2014. Repeated kimberlite magmatism beneath Yakutia and its relationship to Siberian flood volcanism: insights from in situ U–Pb and Sr–Nd perovskite isotope analysis. Earth Planet. Sci. Lett. 404, 283–295. https://doi.org/10.1016/j.epsl.2014.07.039.

Sun, J., Tappe, S., Kostrovitsky, S.I., Liu, C., Skuzovatov, S.Yu., Wu, F., 2018. Mantle sources of kimberlites through time: a U-Pb and Lu-Hf isotope study of zircon megacrysts from the Siberian diamond fields. Chem. Geol. 479, 228–240.

Tappe, S., Foley, S.F., Jenner, G.A., Kjarsgaard, B.A., 2005. Integrating ultramafic lamprophyres into the IUGS classification of igneous rocks: Rationale and implications. J. Petrol. 46, 1893–1900.

Tichomirowa, M., Whitehouse, M.J., Gerdes, A., Götze, J., Schulz, B., Belyatsky, B.V., 2013. Different zircon recrystallization types in carbonatites caused by magma mixing: evidence from U–Pb dating, trace element and isotope composition (Hf and O) of zircons from two Precambrian carbonatites from Fennoscandia. Chem. Geol. 353, 173–198.

Veksler, I.V., Nielsen, T.F.D., Sokolov, S.V., 1998. Mineralogy of crystallized melt inclusions from Gardiner and Kovdor ultramafic alkaline complexes: implications for carbonatite genesis. J. Petrol. 39, 2015–2031.

Vrublevskii, V.V., Voitenko, N.N., Romanov, A.P., Polyakov, G.V., Izokh, A.E., Gertner, I.F., Krupchatnikov, V.I., 2005. Magma sources of Triassic lamproites of Gornyi Altai and Taimyr: Sr and Nd isotope evidence for plume–lithosphere interaction. Doklady Earth Sci. 405a (9), 1365–1367.

Wooden, J.L., Czamanske, G.K., Fedorenko, V.A., Arndt, N.T., Chauvel, C., Bouse, R.M., King, B.-S.W., Knight, R.J., Siems, D.F., 1993. Isotopic and trace-element constraints on mantle and crustal contributions to Siberian continental flood basalts, Noril'sk area, Siberia. Geochim. Cosmochim. Acta 57, 3677–3704. https://doi.org/10.1016/0016-7037(93)90149-Q.

Wu, F.-Y., Yang, Y.-H., Li, Q.-L., Mitchell, R., Dawson, J.B., Brandl, G., Yuhara, M., 2011. In situ determination of U–Pb ages and Sr–Nd–Hf isotopic constraints on the petrogenesis of the Phalaborwa carbonatite Complex, South Africa. Lithos 127, 309–322.

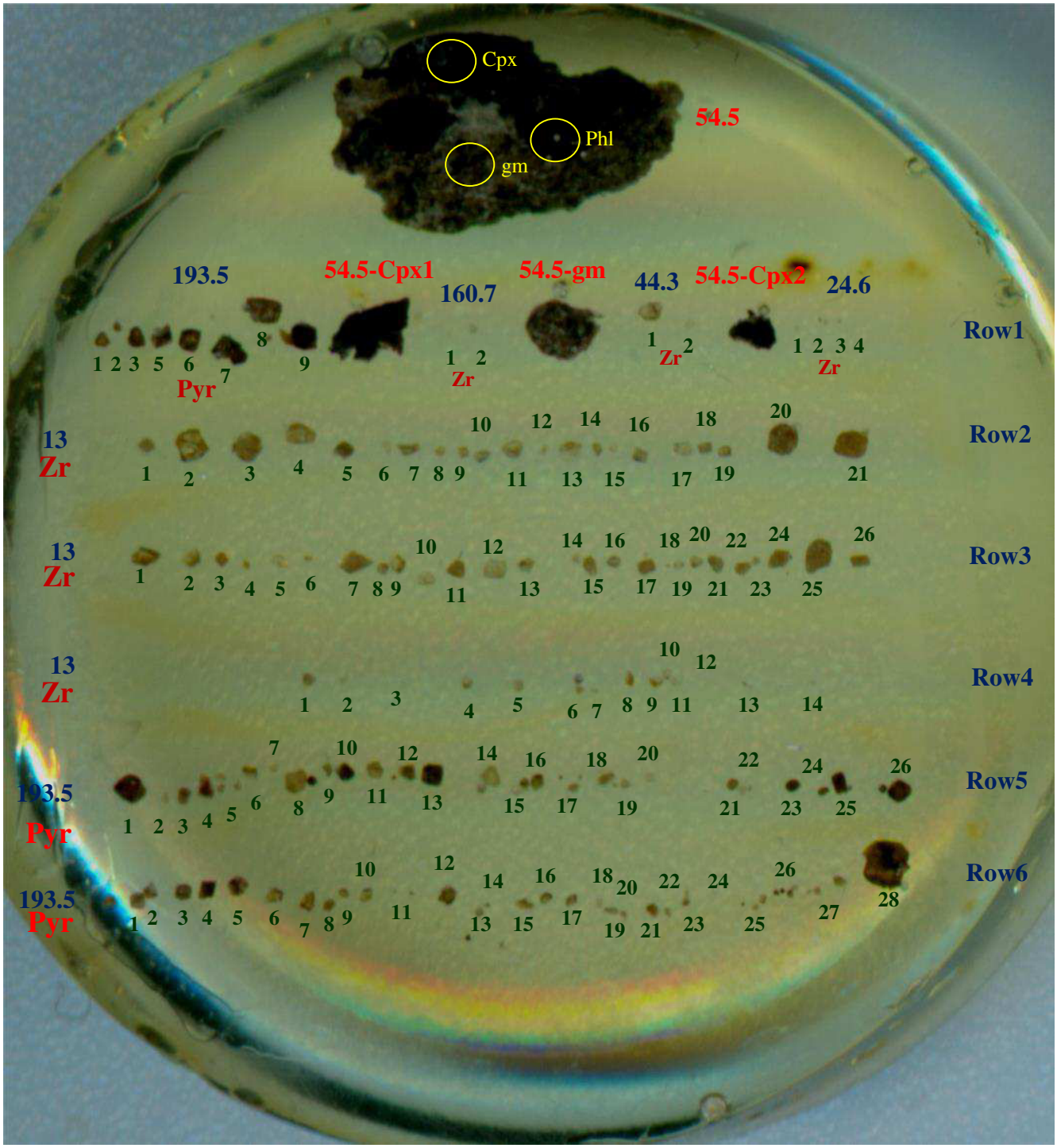

Figure S1. Grains of zircon, pyrochlore and other minerals mounted in epoxy resin, drill holl no.546, Chuktukon intrusion rocks.

Zircons and other minerals were selected from the following depths of the drill hole (in meters, red or blue): 13 – highly weathered damtjernite; 24.6 – weathered damtjernite; 44.3 and 54.5 – damtjernite; 160.7 – hydrothermally overprinted carbonatite; 193.5 – fresh carbonatite.

Symbols: gm – groundmass; Cpx – clinopyroxene; Phl – phlogopite; Pyr – pyrochlore-group minerals; Zr – zircon.

Carbonate matrix of the 546-54.5 sample contains dolomite, calcite, phlogopite, rutile, quartz, K-feldspar, magnetite-magnesioferrite, burbankite, pyrite, various Ni-Co-Cu-Fe-sulfides, cobaltine and illite.

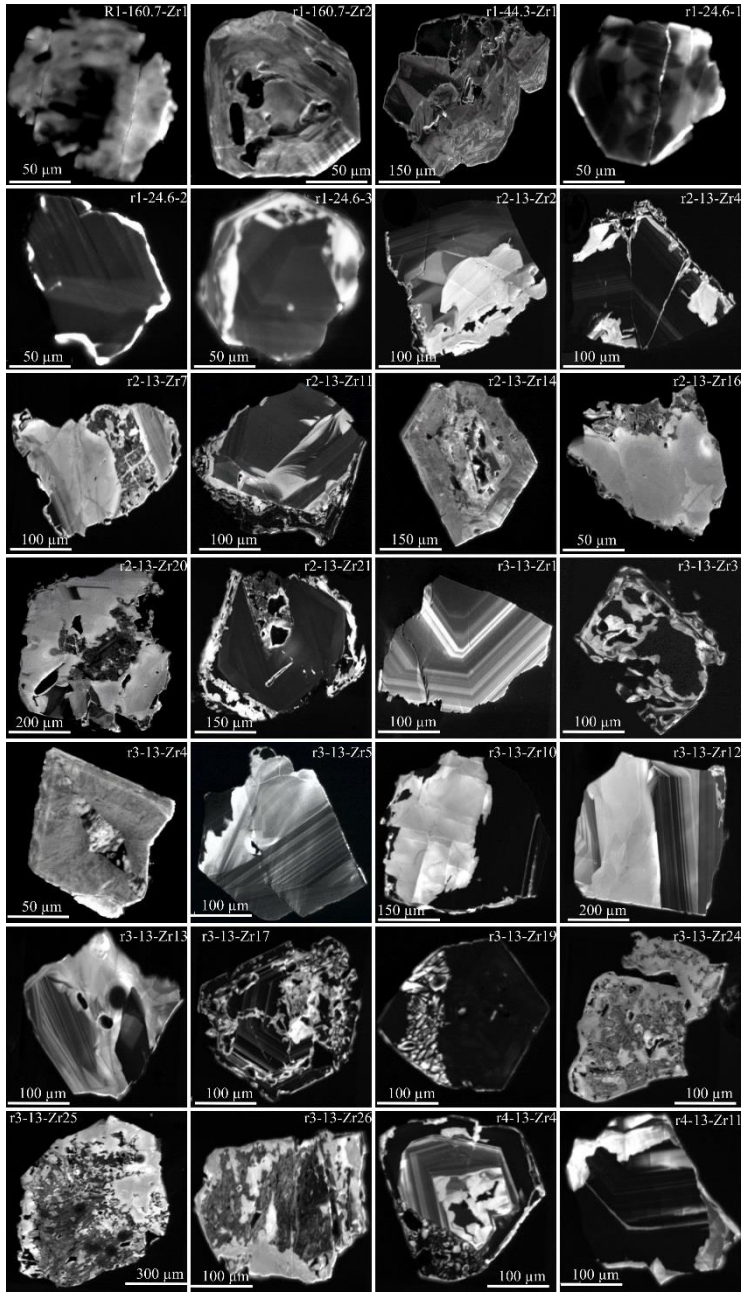

(a)

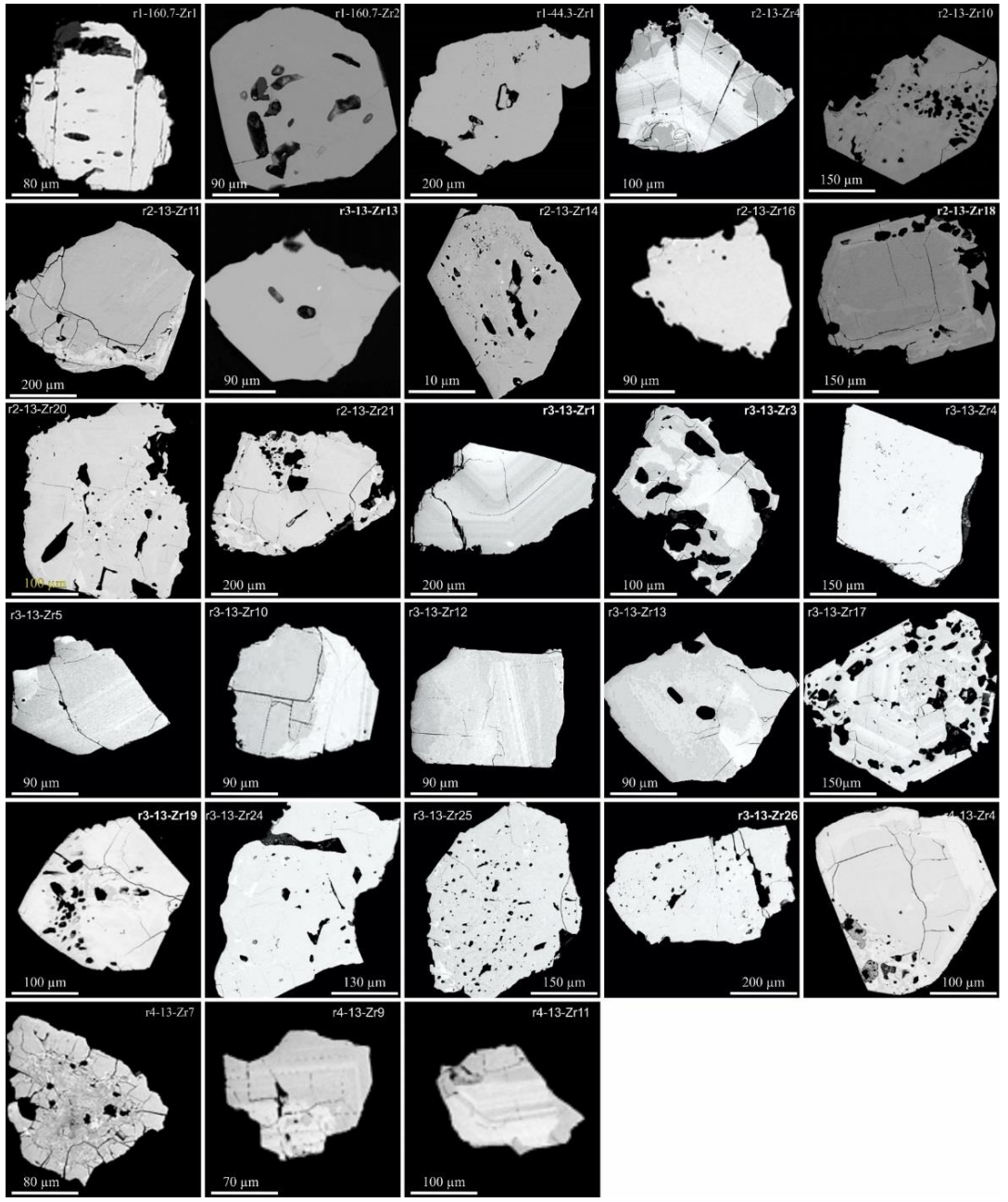

(b)

Figure S2. Representative **(a)** cathodoluminescent (CL) and **(b)** back-scattered electron images (BSE) of zircon grains from drillhole (no. 546) of the Chuktukon complex.

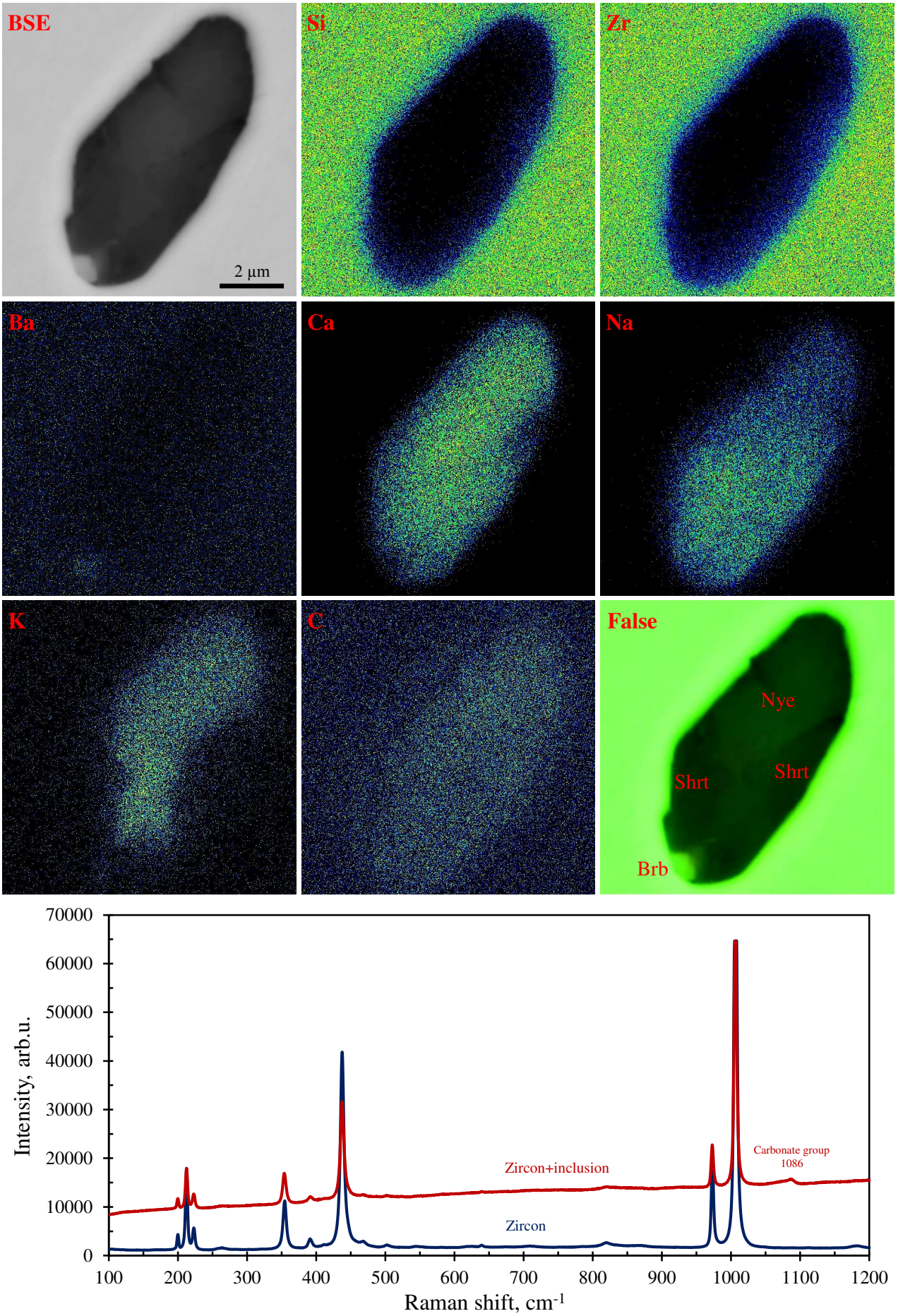

Figure S3. Elemental maps and Raman data for carbonate multiphase inclusion in zircon from calciocarbonatite (depth 160.7 m, drill hole 546), see Fig. 4. Symbols: Nye – nyerereite (?), Shrt – shortite (?), Brb – burbankite (?).

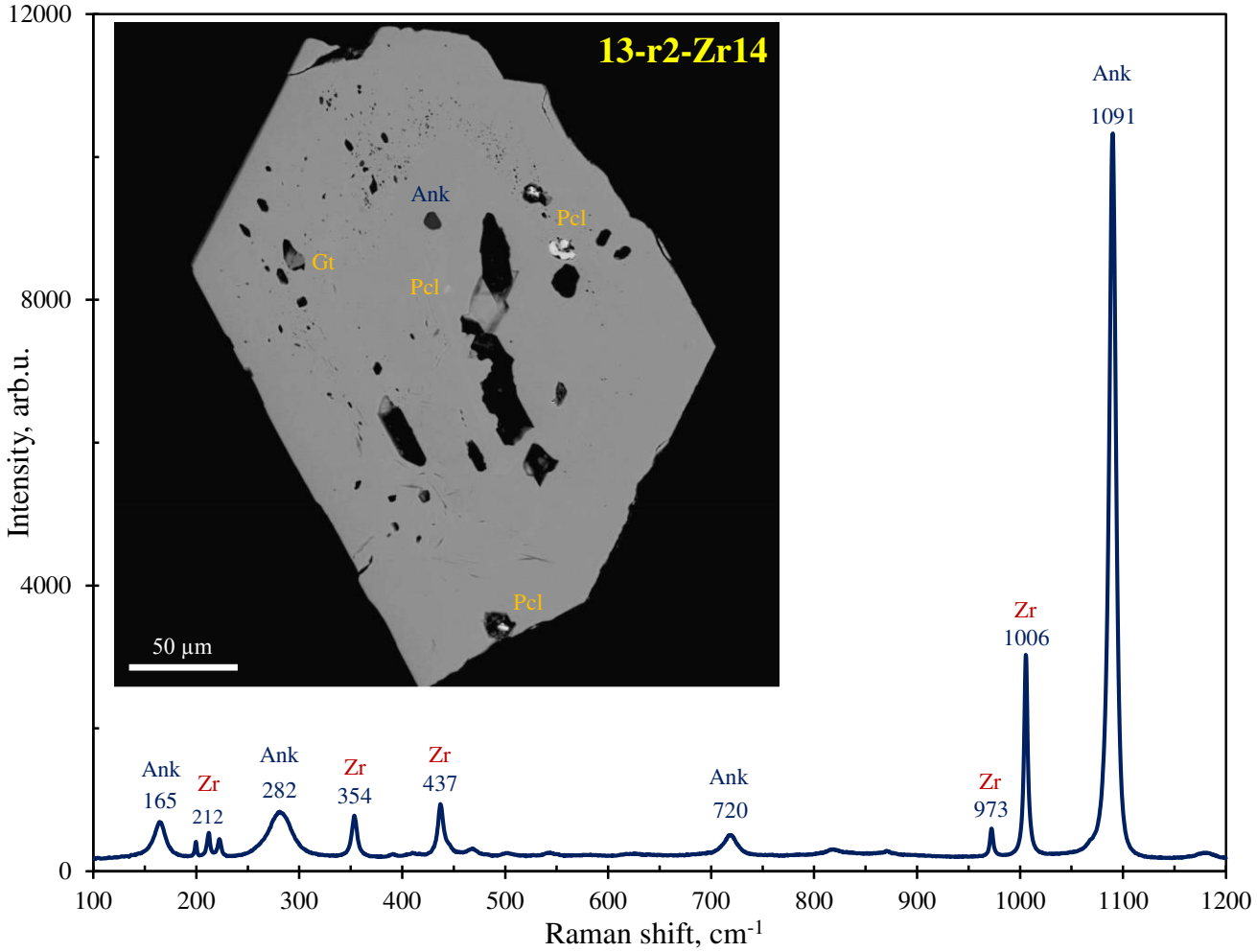

Figure S4. BSE image for a zircon grain from highly weathered damtjernite (depth 13 m, drill holl 546) and Raman spectra for ankerite+zircon. Symbols: Ank – ankerite; Gt – goethite, Pcl – pyrochlore-group minerals; Zr - zircon.
Chemical composition for ankerite (EDS, wt.%): CaO – 26.03; SrO – 0.38; FeO - 18.71; MnO – 4.64; MgO – 6.19.

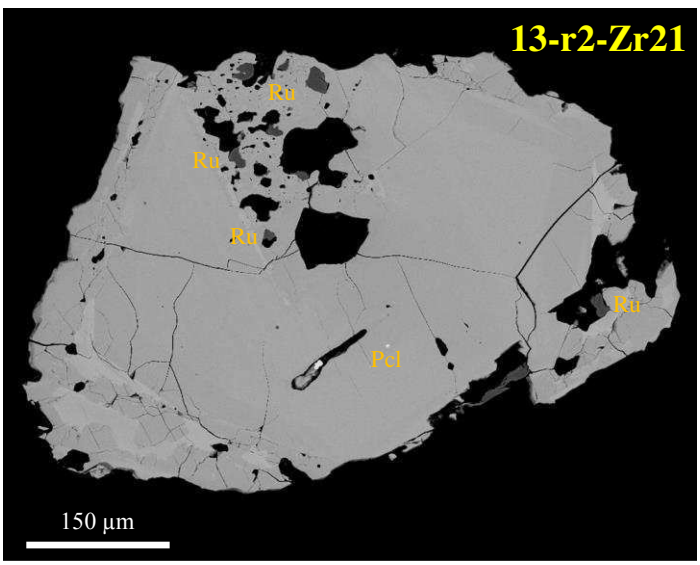

Figure S5. BSE image for a zircon grain containing rutile, highly weathered damtjernite (depth 13 m, drill holl 546). Symbols: Ru – rutile; U-Pcl – U-rich fluorcalciopyrochlore (UO_2 – 12.3 wt.%). Chemical variations for rutile (EDS, wt.%): TiO_2 – 92.7-96.6; Nb_2O_5 – 2.1-5.7; FeO – 0.5-1.4; V_2O_3 – 0.4-0.5.

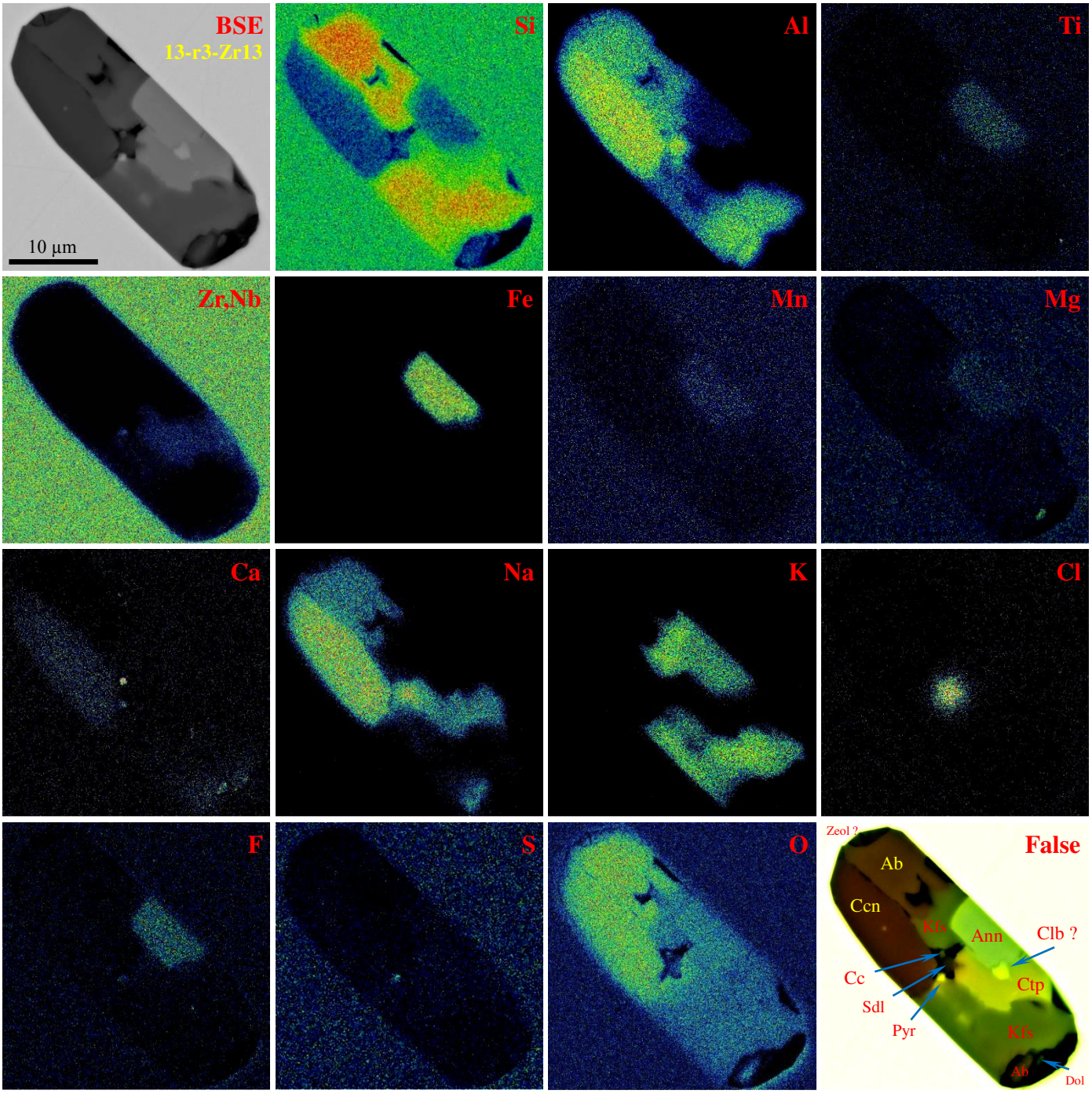

Mineral	*n*	SiO_2	TiO_2	ZrO_2	Nb_2O_5	Al_2O_3	FeO	MnO	ZnO	MgO	CaO	BaO	SrO	Na_2O	K_2O	SO_3	F	Cl	Total
Ab	*2*	68.77				19.32	0.23				0.00	0.00		11.58	0.20				100.10
Kfs	*5*	61.26				18.64	0.45	0.00			0.36	0.26		2.62	12.29				95.89
Ann	*2*	34.23	3.30			10.55	34.29	1.60	0.46	1.91	0.00	0.00		0.23	9.31	0.00	0.00	0.00	95.87
Ctp	*3*	43.01	0.26	31.41	1.27	0.66	1.46				0.21		0.77	12.52	0.75				92.30
Ccn	*2*	36.79				28.54	0.00				2.22	0.00		18.91	0.00	0.45	0.36	0.00	87.27
Sod	*2*	36.15	0.00			25.30	0.52				0.32	0.00		19.50	0.70	0.31	0.00	5.63	88.41

Figure S6. BSE image, elemental maps and mineral chemistry for multiphase inclusion in zircon from highly weathered damtjernite (depth 13 m, drill holl 546). Symbols: Cc – calcite; Ann – annite; Kfs – K-feldspar; Ab – albite; Ccn – a cancrinite-group mineral; Zeol ? – Na-rich zeolite mineral (?); Sdl – sodalite; Pcl – a pyrochlore-group mineral; Ctp – catapleiite; Clb ? – columbite-(Fe) (?). See also Fig. 5. The presence of (OH)-group or H_2O in annite, cancrinite and catapleiite is supported by Raman bands in the 3000-3900 cm^{-1} region.

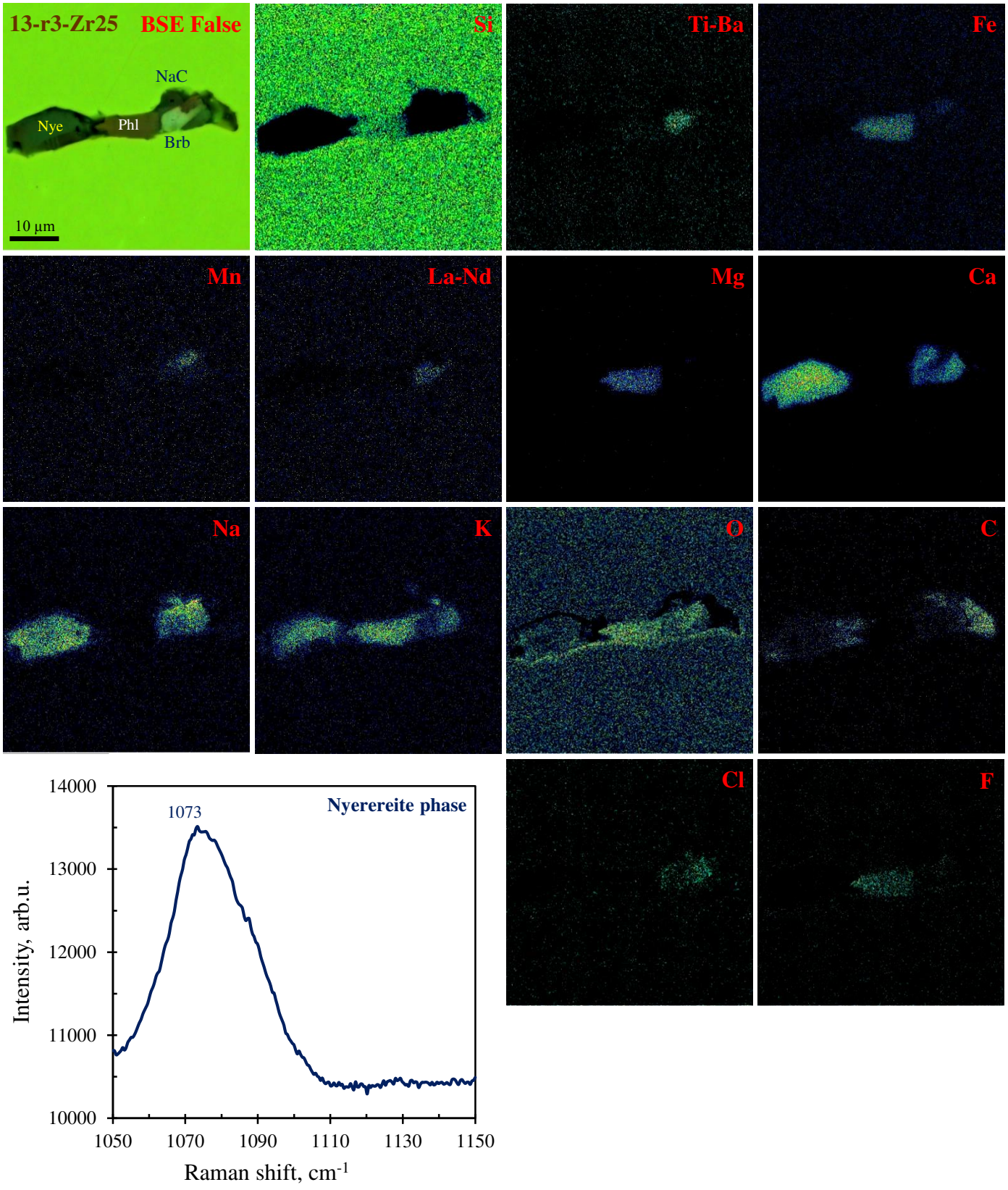

Figure S7. BSE image, elemental maps and Raman spectra for "nyerereite" for multiphase inclusion in zircon from highly weathered damtjernite (depth 13 m, drill holl 546). Symbols: Nye - "nyerereite"; Phl – phlogopite; NaC – hydrated Na-rich carbonate; Brb – burbankite.. See also Fig .6.
Chemical composition for nyerereite phase (EDS, wt.%): CaO – 26.63; SrO – 0.67; FeO – 0.00; Na2O – >14.64; K2O – 6.42. The nyerereite phase is party hydrated, it is fixed due to the presence of weak Raman band near 3150 cm^{-1}.

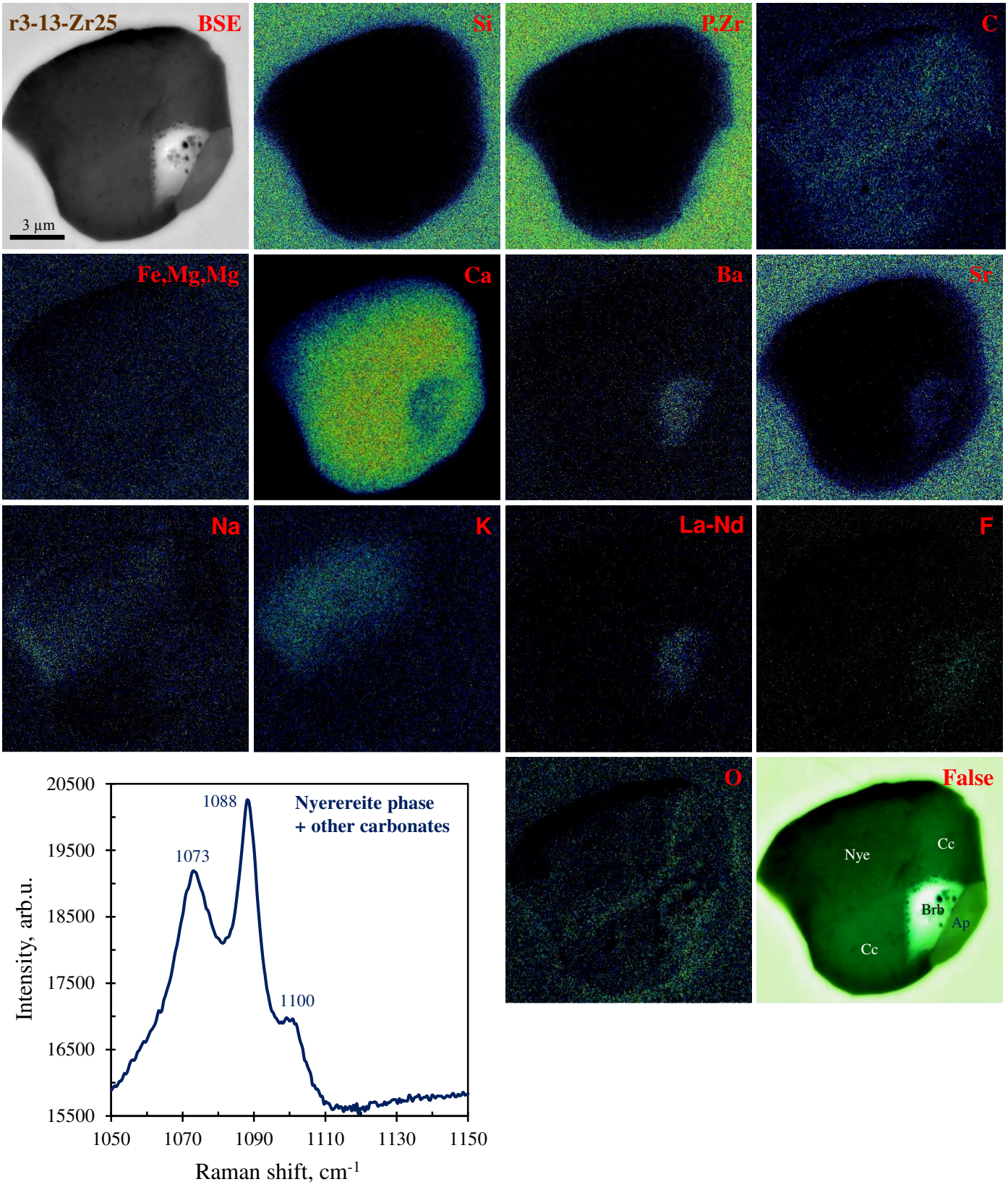

Figure S8. BSE image, elemental maps and Raman spectra for "nyerereite" for multiphase inclusion in zircon from highly weathered damtjernite (depth 13 m, drill holl 546). Symbols: Nye - "nyerereite"; Cc – calcite; Ap – fluorapatite; Brb – burbankite- khanneshite. See also Fig .6.

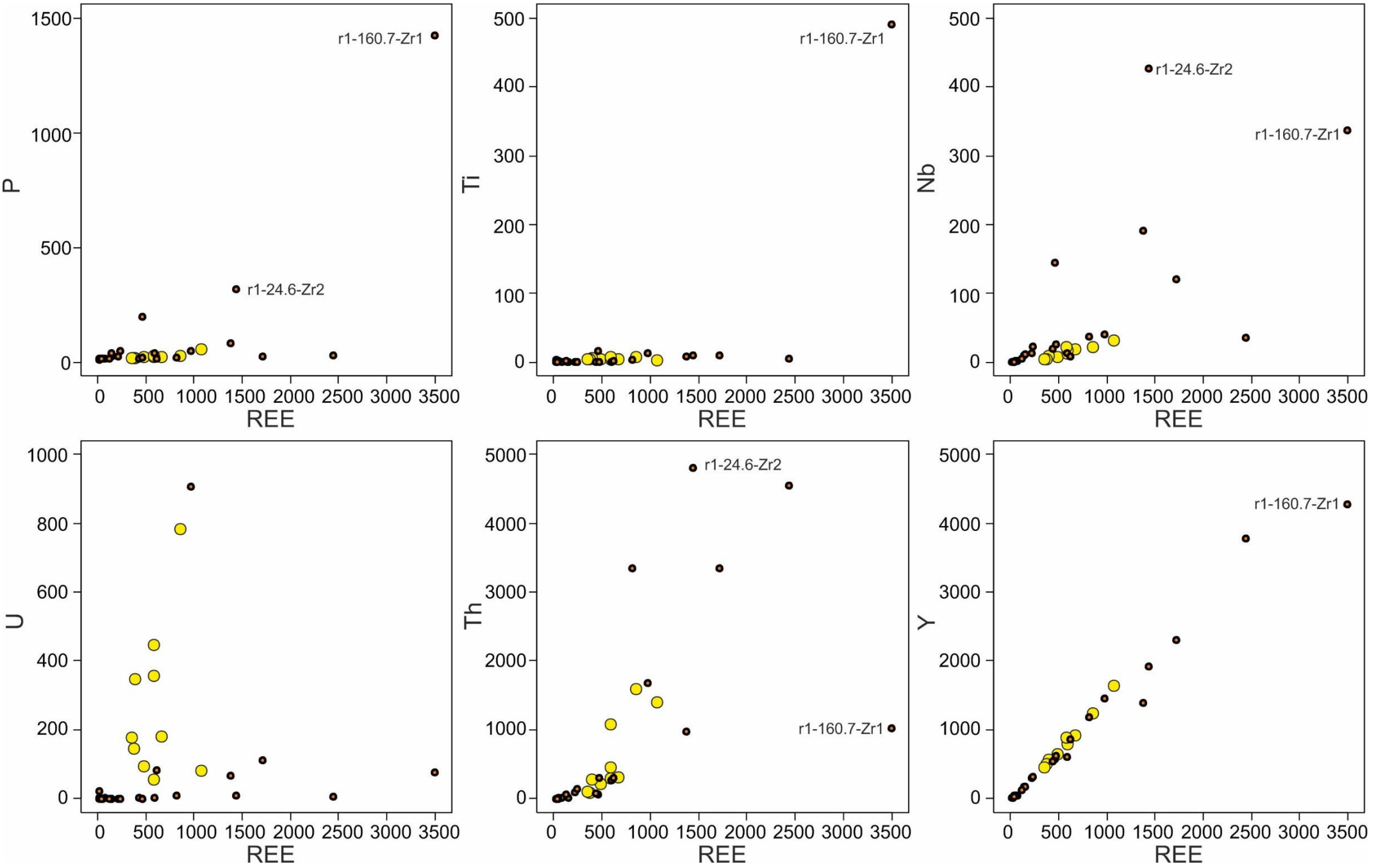

Figure S9. Trace element characteristics of zircons with oscillatory and sectorial zoning (yellow circles) and with signatures of recrystallization (orange circles).